Seismic Performance Investigation of the Folded Cantilever Shear Structure Which Consists of Fixed and Movable Sub-Frames

PhD Thesis

August, 2013

Ercan Serif KAYA

Graduate School of Science and Technology

KUMAMOTO UNIVERSITY

Abstract

A newly designed structure named folded cantilever shear structure (FCSS) is proposed as an alternative seismic isolation approach incorporating coupling method and base isolation method in one structure for improving earthquake resistant ability and seismic performance of mid-rise buildings. The proposed structure consists of non-isolated, which is named fixed, and fully isolated, which is named movable, sub-frames of similar heights, and these fully separated sub-frames were rigidly connected to each other by a connection sub-frame at the top part. This allows all three sub-frames to behave as a unique structure. In this manner, it is aimed to extend the natural period of the structure and to decrease the overall seismic responses.

It was found that the proposed structure is capable of extending natural period and minimizing accelerations, displacements and base shear forces simultaneously, when compared to ordinary structure which has the same number of storey. However, relative displacements, for the proposed structure without additional dampers, with respect to the base were obtained relatively higher. Therefore, additional viscous dampers were added between adjacent beams to connect both sub-frames with the aim of avoiding excessive displacements and increasing the damping ratio as well. In this dissertation, dynamic characteristics of the proposed structure have been investigated theoretically and experimentally.

In chapter 1, a brief introduction about the previous works on coupled structures and coupling configurations are given.

In chapter 2, the detailed dynamic characteristics of an ordinary mid-rise building are introduced by reason of the ordinary building is taken as a comparison model for the proposed building. By taking both structure with similar height and characteristics, it is possible to explore whether the proposed model has shown any enhancement in terms of seismic performance.

In chapter 3, the proposed building named, folded cantilever shear structure, is introduced. The design principles and building configuration is elaborated by illustrative figure. Then the detailed dynamic characteristics of the proposed building are introduced for two different cases which are; folded cantilever shear structure without and with additional dampers. Simple equations are also derived to let us estimate the dynamic parameters of the proposed building for

a given parameters. And natural frequencies, damping ratios, mode shapes and their relations with storey number is investigated.

In Chapter 4, numerical studies were conducted in order to verify the dynamic parameter characteristics and the theory of the proposed structure that is elaborated in the previous chapter. Three models, ordinary building and proposed building without and with additional dampers, were investigated through eigenvalue analysis and elastic dynamic response analyses under four exemplary ground motions, namely El Centro, Hachinohe, Miyagi and Taft earthquakes. The preliminary results were obtained confirming that the structural behaviour and seismic performance is upgraded in case of proposed model.

In Chapter 5, the seismic behaviour investigation of the proposed structure is elaborated by applying a set of experiments to obtain dynamic parameters such as natural frequencies, damping ratios and mode shapes. Shaking table test were also conducted by using 16-storey vibration model under same ground motions used in numerical studies. Since the experimental vibration model is not a scaled model, the results were also compared and verified by analyzing experimental vibration model on ABAQUS, well-known finite element software. In both studies, the proposed structure performed substantial improvement in reducing seismic responses when compared to ordinary structure of similar height.

In chapter 6, the proposed structure is modified to come up with an idea avoiding structural irregularity with a symmetrically designed building of FCSS consisted fixed - movable - fixed sub-frame configuration. Similar to the first configuration of the proposed structure, the seismic behaviour of the modified model is elaborated due to numerical and experimental analysis. In general terms, the modified structure provides better outcomes such as symmetrical configuration, providing more space for damping placement and better seismic performance. Therefore, the modified model is set as the final configuration of proposed structure to be vibration model for the numerical studies of real-scale building investigations to be design as mid-rise building. This modified model is also tested through numerical and experimental analyses to clarify whether it has an increasing effect on seismic performance or not when compared to old type of fcss which has only two sub-frame configuration, fixed - movable sub-frames. An introduction to real-scale building investigations are given, including the preliminary seismic behaviour studies on the real-scale model.

In Chapter 7, conclusion is given.

Acknowledgements

Foremost, I would like to express my deep and sincere gratitude to my supervisor Prof. Toshitaka Yamao for his continuous support and encouragement of my PhD research, his patience, kindness and valuable ideas made this thesis possible. He always has been more than a supervisor for me with his great supports.

Beside my supervisor, I also would like to express my great gratitude and appreciation to Prof. Takuro Katayama. His guidance helped me all in the time of my research. His hard work, kind and endless support motivated me all along of this thesis.

I would like to express my gratitude and acknowledge the dissertation committee members, Prof. Taiji Mazda and Prof. Akira Kasai and Koji Ogawa for their useful suggestions for my research and tremendous help in aspect of the final version of my thesis for correcting and offering suggestions for improvement, and also thank to Prof. Minori Yamanari for his sincere and endless support for my simulation studies.

I thank my old and current fellow labmates in Structural Dynamics Lab for the stimulating discussions, their valuable helps in the last three years. Also I thank my friends who accompanied me during the time I live in Kumamoto and who will keep doing so.

I would like to express my great appreciation and respect to the Department of Architectural and Civil Engineering, Kumamoto University for hosting me and providing this priceless opportunity.

I owe a great debt to the Ministry of Education, Culture, Sports, Science and Technology, for the generosity in funding. I have been greatly honoured to be a recipient who awarded for the Japanese Government Scholarship. I am extremely grateful for the Japanese Government for the confidence and willingness to help me achieve my career goals.

Last, I would like to thank my family: my parents Ayse Kaya and Mesut Kaya for their eternal love and for supporting me spiritually throughout my life.

Contents

List of Tables

List of Figures

CHAPTER 1

Introduction

In the last decade, coupling method has received increasing attention by a significant amount of researchers dealing with structural responses and pounding issues of mid-rise structures due to seismic and wind excitations. One of the main aspects of this concept is that the method let researchers interconnect adjacent structures by incorporating various passive energy dissipation devices and base isolation systems in structures. Moreover, coupling method is also similar to base isolation method in that it can be implemented either in existing or newly designed structures not only for reducing pounding possibility but also increasing seismic performance.

For instance, Ohami *et al.* [1] tried to improve the seismic reliability of an existing structure built in accordance with old provisions of building codes of Japan before revisions were made in 1981. Different heights of buildings, one is 5-storey representing old building and the other is 10-storey building representing newly designed building, were selected to be idealized shear models for numerical analysis, and interconnections were made by using rigid connection elements and viscous dampers. The reason for choosing buildings of different heights was reported that responses of coupled buildings could not be reduced when similar heights of buildings was chosen, Azuma *et al.* [2] and Ohami *et al.* [1]. As a result, it was found that it is more effective to design new building to be connected to old one as stiff building instead of flexible building when rigid connection elements were used and rigid connection elements were insufficient to prevent the collapse of 5-storey old building when incorporated in flexible building. In another remarkable study, Ng and Xu [3] carried out an experimental investigation using 12-storey building model to be interconnected to 3-storey low-rise podium structure in 3 different configurations which are respectively fully-separated, rigidly connected and friction damped-linked. Results showed that passively controlled buildings provided most effective performance when compared to other cases. Interestingly, the rigidly connected buildings gave rise to increase in seismic responses. Xu *et al.* [4] also stated that fluid damper connected buildings are more effective in reducing seismic responses for lower adjacent buildings than of higher ones and fluid dampers are more favorable for buildings of same height than those of different heights. Some selected studies with similar configurations and outcomes can be seen in these references, Luco and Barros [5] and Cimellaro *et al.* [6]. As seen in these studies, it should be noted that most of researches headed for studying coupling method on buildings of different heights, but it should also be taken into account that most of them used boundary conditions of each buildings to be fixed as well.

Aida *et al.* [7] used only one connecting member which consists of one spring and one damper element to connect adjacent structures of different heights, one structure is n-dof and the other is m-dof, for improving damping performance. Numerical results showed that the most effective position to place connecting member was near to the top part of the structures and the damping performance increased as long as first natural periods of the structures became different. Hysteretic dampers were also used as connecting element in another study between two mdof structures by Basili and Angelis [8]. Three cases were considered for numerical studies, two 10-storey structures connected at their roofs, and as for structures of different heights, one flexible 20-storey structure connected to the roof of a stiff 10-storey structure and 4-storey structure connected to the roof of a stiff 2-storey structure. In all cases, single hysteretic damper element used as a connector element, and also same structures analyzed for non-connected and rigidly-connected cases to compare the responses of the structures for different type of connections. Example results show that the hysteretic damper connection was more effective in reducing seismic responses for the structures of similar heights when compared to rigidly-connected and non-connected structures. As for structures of different heights, it was pointed out that the rigid connection performed a negative effect on protection of lower structure. It is also stated that rigid connection device does not appear as a convenient solution for such adjacent structures.

Agarwal *et al.* [9] in their study that the most common foundation configuration is that with both buildings fixed and they gave the reason for this as that base isolation is a relatively new response modification technique. Therefore, they investigated pounding responses of two adjacent buildings of similar heights with friction varying base isolation. Three different configurations for these two buildings were used for this purpose namely, single base isolated building, and buildings with and without base isolation systems with varying coefficient of friction. According to the results, there was little or no interaction between buildings for the case of single base isolated building configuration.

Besides, shared tuned mass damper was implemented as an alternative connection element to adjacent by Abdullah *et al.* [10] in reducing vibration and pounding in adjacent structures. Moreover coupling method can be used for special cases such as over-track buildings, Hayashi [11] and Iwasaki *et al.* [12] for better use of space in high density cities.

In the view of these studies, there are few common points to be underlined that can be summarized as: (i) coupling method can be an effective solution to deal with the problem of not only pounding but also decreasing seismic responses of mid-rise buildings, (ii) However, most researchers have used buildings of different heights configuration to be modelled with fixed boundary conditions, (iii) rigid connections have not been preferred as connecting elements when coupling buildings of similar heights due to insufficient outcomes in reducing building responses. Therefore, viscous damping devices come up with more favourable results.

The main objective of this study is to propose an alternative seismic isolation approach incorporating base isolation system and coupling method into a mid-rise structure with the aim of increasing seismic performance and natural period. Therefore, a new configuration for buildings of similar heights were proposed and studied by connecting them at the roof part. Contrary to common configurations as above mentioned researches, the boundary conditions were selected to be one fixed supported building and the other to be base isolated building while using rigid connection at the top part, and buildings were also selected to be similar heights.

A standard acceleration response spectrum of an ordinary structure with 5% damping ratio is given in Figure 1.1. The natural period of an ordinary mid-rise structure is likely to be around 1 sec. And as expected, the acceleration of the structure reduces as long as period increases. As for the proposed structure named folded cantilever shear structure (FCSS), it is able to extend the first natural period almost two times when compared to ordinary folded cantilever shear structure (OCSS), by increasing the floor number by a factor of two without changing the total height of structure. For this purpose, the proposed structure is designed consists of three main parts, namely, fix-supported shear sub-frame, movable shear sub-frame which is supported by roller bearings and connection sub-frame at the top part connecting these sub-frames to each other and uniting them as one structure. Besides, adjacent beams of sub-frames were connected to each other by additional viscous dampers to avoid excessive displacements and to increase the damping ratio as well.

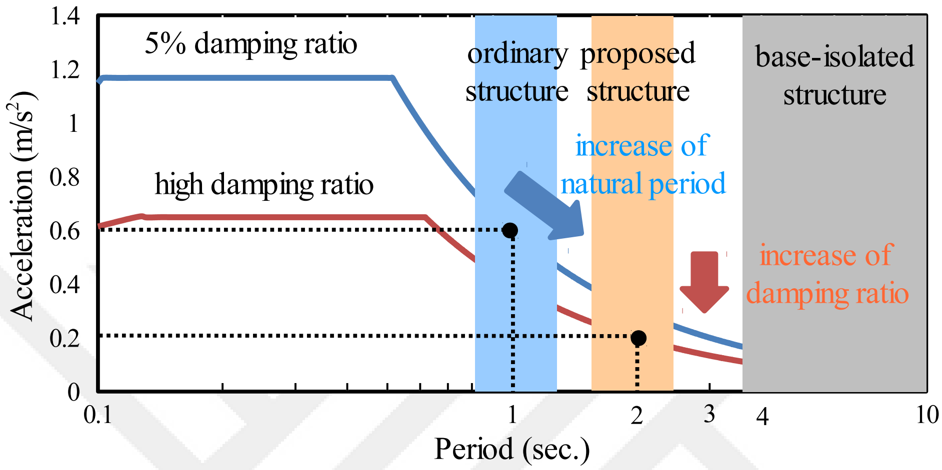

Figure 1.1: Standard acceleration response spectrum (increasing period and damping ratio)

In order to elaborate the studies, numerical investigations and a set of experimental investigations were conducted to obtain dynamic parameters and shaking table responses by using vibration model of the proposed structure with and without additional dampers. As for additional damper added structure, some studies offers practical and effective damper placement methods such as Garcia [13], Luco and Barros [5]. And Whittle *et al.* [14] compared these methods in their study terms of effectiveness. Despite of these methods' benefits, these techniques are for advanced optimization, and the vibration model in this study, with additional dampers case, assumed to be uniformly distributed to clarify whether the newly designed structure is effective in reducing seismic responses.

CHAPTER 2

Dynamic Characteristics of an Ordinary Mid-Rise Buildings

2.1 Introduction

In this chapter, dynamic characteristics of an ordinary mid-rise building are given on the basis of vibration theory. First of all, some simple equations are derived that let us estimate the dynamic parameters of an ordinary shear structure such as natural period, damping ratio of an n storey ordinary structure, which is a multi degree of freedom, $mdof$ system, by using inter-storey parameters of the same structure which can be assumed as a single degree of freedom, $sdof$ system. Since the ordinary building is set as a comparison model for the proposed building, the results for the numerical studies will compared to ordinary study. By doing so, the structural enhancement can easily predicted.

2.2 Ordinary mid-rise building

Figure 2.1 illustrates a two-dimensional vibration model of an ordinary multi-storey shear structure. The vibration model, named as System-O, has fixed end consisting n number of storey. Beams are represented as B_1, B_2, $\cdots$ B_n, and columns and dashpots are identical in terms of dynamic characteristics for each storey. The letter m stands for the mass of beam, k is the shear spring coefficient of column and c is the viscous damping coefficient of dashpot to represent the structural damping of idealized vibration model.

The total height of the n-storey vibration model is H and each storey has a height of h, $H = nh$. The beams are carrying the concentrated masses of beams and columns at their center.

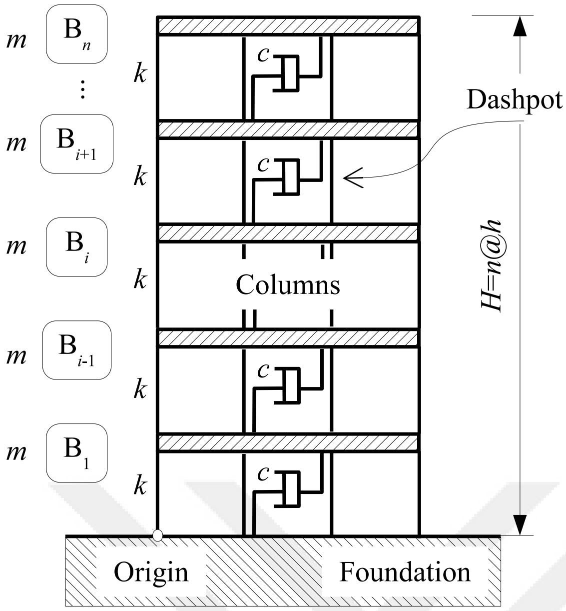

Figure 2.1: Ordinary structure (Sytem-O)

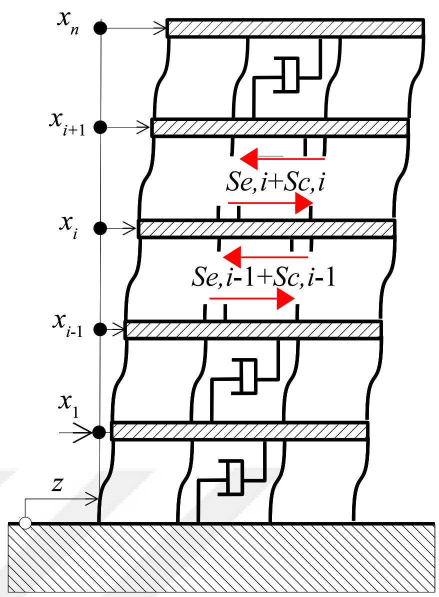

Figure 2.2: Deformed frame of System-O

2.2.1 The equation of motion of an ordinary building under base excitation

The deformed frame and the internal forces of System-O due to displacement excitation are illustrated in Figure 2.2, under $z(t)$ time-varying ground motion, where z is the relative displacement of the base from its origin and x_1, x_2, $\cdots$, x_n are the lateral displacements of beam B_1, B_2, $\cdots$, B_n. The relative displacement for the i-th storey, B_i, is $z + x_i$ whereas shear and viscous damping forces between beam B_i and B_{i+1} are represented as S_e, i and S_c, i, respectively. The inertia force of beam B_i is also represented as S_m. The equilibrium of the forces of beams are become as following equation;

$$\begin{aligned} -S_{m,i} + S_{c,i} - S_{c,i-1} + S_{e,i} - S_{e,i-1} = 0 \qquad 1 \leq i < n \\ -S_{m,n} - S_{c,n-1} - S_{e,n-1} = 0 \end{aligned} \tag{2.1}$$

The shear, viscous damping and the inertia forces between the beams can be expressed as $S_{e,i} = k(x_{i+1} - x_i)$, $S_{c,i} = c(\dot{x}_{i+1} - \dot{x}_i)$ and $S_{m,i} = c(\ddot{z} + \ddot{x}_i)$, respectively where $\dot{x}_i$ and $\ddot{x}_i$ stands for the first and second derivation of displacement, x_i. And $\ddot{z}$ is the acceleration of the ground.

With respect to ground floor, shear and damping forces of the beam can be expressed as $S_{e,0} = k(x_1)$ and $S_{c,0} = c(\dot{x}_1)$, respectively. After substituting these equations of the forces into Eq. 2.1, the equation of the motion of System-O due to lateral displacement excitation becomes as the following equation;

$$M^{(n)}\ddot{x}^{(n)} + C^{(n)}\dot{x}^{(n)} + K^{(n)}x^{(n)} = -\ddot{z}M^{(n)}p^{(n)} \tag{2.2}$$

Where, $p^{(n)}$ is the column vector which has all its elements equal to 1. And $x^{(n)} \equiv [x_1, x_2, \cdots, x_n]^T$, $\dot{x}^{(n)} \equiv [\dot{x}_1, \dot{x}_2, \cdots, \dot{x}_n]^T$ and $\ddot{x}^{(n)} \equiv [\ddot{x}_1, \ddot{x}_2, \cdots, \ddot{x}_n]^T$ are the displacement, velocity and acceleration vectors, respectively. The letter (n) denotes the size of square matrices for n number of storey and T stands for transverse.

$$K^{(n)} = kQ^{(n)} \tag{2.3a}$$

$$C^{(n)} = cQ^{(n)} \tag{2.3b}$$

Besides, Eq. 2.3c is the mass matrix $M^{(n)}$ where $I^{(n)}$ is the unit matrix and m is the mass.

$$M^{(n)} = mI^{(n)} \tag{2.3c}$$

$$Q^{(n)} \equiv \begin{bmatrix} 2 & -1 & 0 & \cdots & 0 \\ -1 & 2 & -1 & \ddots & \vdots \\ 0 & \ddots & \ddots & \ddots & 0 \\ \vdots & \ddots & -1 & 2 & -1 \\ 0 & \cdots & 0 & -1 & 1 \end{bmatrix} \tag{2.4}$$

Eq. 2.3a and Eq. 2.3b show the n size of square matrices of Eq. 2.2 where $K^{(n)}$ and $C^{(n)}$ are the stiffness and damping matrices obtained by the tri-diagonal constant matrix, $Q^{(n)}$ of Eq. 2.4 with shear spring constant, k and viscous damping coefficient, c.

2.2.2 Natural period characteristics

A simple equation is derived that let us estimate the natural period of the n storey ordinary structure of Figure 2.1, a $mdof$ system, by using inter-storey parameters of the same structure which can be assumed as a $sdof$ system.

$$\bar{T} = \frac{2\pi}{\bar{\omega}} \equiv 2\pi\sqrt{\frac{m}{k}} \tag{2.5a}$$

$$\bar{\zeta} \equiv \frac{c}{2\sqrt{mk}} \tag{2.5b}$$

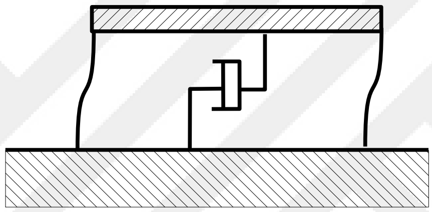

Figure 2.3: Inter-storey section of System-O

Note that the letters with overhead bars of Eqs. 2.5a and 2.5b such as, natural period $\bar{T}$, damping ratio $\bar{\zeta}$, and natural frequency $\bar{\omega}$ are the parameters of inter-storey of System-O, Figure 2.3, that can be calculated by means of basic equations of structural dynamics.

The eigenproblem of the undamped structure of System-O becomes;

$$(K^{(n)} - \omega^2 M^{(n)})\varphi^{(n)} = 0 \tag{2.6a}$$

Here, ω and $\varphi^{(n)}$ are the natural frequency and corresponding eigenvector. Eq. 2.6a after substituting Eq. 2.3a and Eq. 2.3c becomes standard eigenvalue problem;

$$(Q^{(n)} - \lambda^2 I^{(n)})\varphi^{(n)} = 0 \tag{2.6b}$$

where λ is the eigenvalue. The natural frequency ratio λ_i, gives the ratio between the natural frequency of vibration model ω_i, and natural frequency of inter-story $\bar{\omega}$. Besides, the natural period of the vibration model T_i, and natural period of inter-story $\bar{T}$ becomes;

$$\lambda_i = \frac{\omega_i}{\bar{\omega}} = \frac{\bar{T}}{T_i} \tag{2.7}$$

The eigenvector $\varphi_i^{(n)}$ is normalized to satisfy the orthogonal condition and δ_{ij} is treated as Kronecker delta, Eq. 2.8a and Eq. 2.8b.

$$\varphi_i^{(n)T} Q^{(n)} \varphi_j^{(n)} = \delta_{ij}\lambda_i^2 \tag{2.8a}$$

$$\varphi_i^{(n)T} \varphi_j^{(n)} = \delta_{ij} \tag{2.8b}$$

Numerical equations of natural frequency ratio λ_i and eigenvector $\varphi_i^{(n)}$ become;

$$\lambda_i = 2sin\left(\frac{2i-1}{4n+2}\pi\right), \qquad 1 \leq i \leq n \tag{2.9}$$

$$\varphi_i^{(n)} \equiv \left[\phi_{1,i}^{(n)}, \phi_{2,i}^{(n)}, \cdots, \phi_{n,i}^{(n)}\right]^T \tag{2.10a}$$

$$\phi_{j,i}^{(n)} = \frac{2}{\sqrt{2n+1}} sin\left(\frac{2i-1}{2n+1}j\pi\right) \tag{2.10b}$$

After proportioning the Eq. 2.7 and Eq. 2.9, the ratio between the natural period of the vibration model and of inter-story can be estimated,

$$\frac{T_i}{\bar{T}} = \frac{1}{2}cosec\left(\frac{2i-1}{4n+2}\pi\right), \qquad 1 \leq i \leq n \tag{2.11}$$

An approximate equation becomes as in follows of the first natural period on the basis of Eq. 2.11 in case that $1 \ll n$,

$$T_1 \approx \frac{\bar{T}}{\pi}(2n+1) \tag{2.12a}$$

That is, the first natural period of structure can be extended as long as the number of storey n, increases for a specified natural period of inter-storey $\bar{T}$. The primary natural period for design use of the building can be calculated by following equation due to the Building Standard Law of Japan [15].

$$T_1 = \eta H \tag{2.12b}$$

where η, is specified respectively as 0.03 and 0.02 for steel and reinforcement structures, the Building Standard Law of Japan. Therefore, the first natural period is likely to be around 1 sec for mid-rise buildings of $40 \sim 60\ m$ height. After proportioning the right sides of the Eq. 2.12a and Eq. 2.12b, the approximate equation of inter-storey for the first natural period becomes;

$$\bar{T} \approx \frac{\pi \eta h}{2 + 1/n} \tag{2.13}$$

These approximate equations' results will be compared to the results of numerical analyses using given parameters of illustrative example.

2.2.3 Viscous damping characteristics

The equation of viscous damping ratios of the vibration model and of inter-story becomes as in Eq. 2.14 by using the eigenvector of System-O, $\varphi_i^{(n)}$ and viscous damping ratio due to orthogonality condition of Eq. 2.10a and Eq. 2.10b.

$$\frac{\zeta_i}{\bar{\zeta}} = \lambda_i = 2sin\left(\frac{2i-1}{4n+2}\pi\right), \qquad 1 \leq i \leq n \tag{2.14}$$

An approximate result can be obtained by derived Eq. 2.14 in case that, $1 \ll n$ for the first natural vibration vector,

$$\zeta_1 \approx \frac{\pi\bar{\zeta}}{2n+1} \tag{2.15a}$$

If the viscous damping ratio of the System-O is estimated for a specified $\bar{\zeta}$ the viscous damping ratio of the first mode is decreased as long as the number of storey, n increases. Considering, the viscous damping ratio of first mode of steel and reinforcement structures are around $1\% \sim 5\%$, and the relation between the structure height and the viscous damping ratio can be obtained after substituting the estimated viscous damping ratio ζ_1^*, into Eq. 2.15a

$$\bar{\zeta} \approx \frac{2n+1}{\pi}\zeta_1^* \tag{2.15b}$$

2.3 Conclusion

In this chapter, dynamic characteristics of an ordinary mid-rise building is given. Simple equations are derived to estimate dynamic parameters of $mdof$ system by using $sdof$ system parameters. Derivated equations will be used for the numerical analysis in order to compare the dynamic parameter results with of proposed building model.

CHAPTER 3

Dynamic Characteristics of Folded Cantilever Shear Structure

3.1 Introduction

The main objective of the proposed building is to extending the first natural period almost two times by increasing the floor number by a factor of two in such a way that neither the number of storey n, nor structural height of ordinary structure H, has been altered. Therefore it is designed as an assembly of three different parts in one structure as seen Figure 3.1. The vibration model consists of a fix-supported shear sub-frame and movable shear sub-frame supported by roller bearings. These sub-frames are interconnected by a rigid connection frame at the top of the structure to enable separated sub-frames to move together as unique structure during any excitation. In brief, it can be assumed that a $2n$-storey of ordinary structure with the height of $2H$ is equalized to n-storey of proposed structure with the height of H. As mentioned in abstract, the numerical analyses were conducted on the idealized vibration model with and without additional viscous dampers. The vibration model given in Figure 3.1 is named as System-AD since its additional dampers attached between the adjacent beams of fixed and movable sub-frames against excessive displacements. Beams were named as B_1, B_2, $\cdots$, B_{i-1}, B_i, B_{i+1}, $\cdots$, B_{n-1} starting from the fixed shear sub-frame. Then, the uppermost rigid connection beam was named as B_n. On the side of movable sub-frame, beams were continued to be named as B_{n+1}, B_{n+2}, $\cdots$, B_{j-1}, B_j, B_{j+1}, $\cdots$, B_{2n} Beam-$2n$ is the one that is supported by roller bearings and it can move along x and z directions.

The beams are carrying the concentrated masses of beam and columns at their center, and m_A represents the lumped masses of beams starting from beam-1 to beam-$(n-1)$ on the side

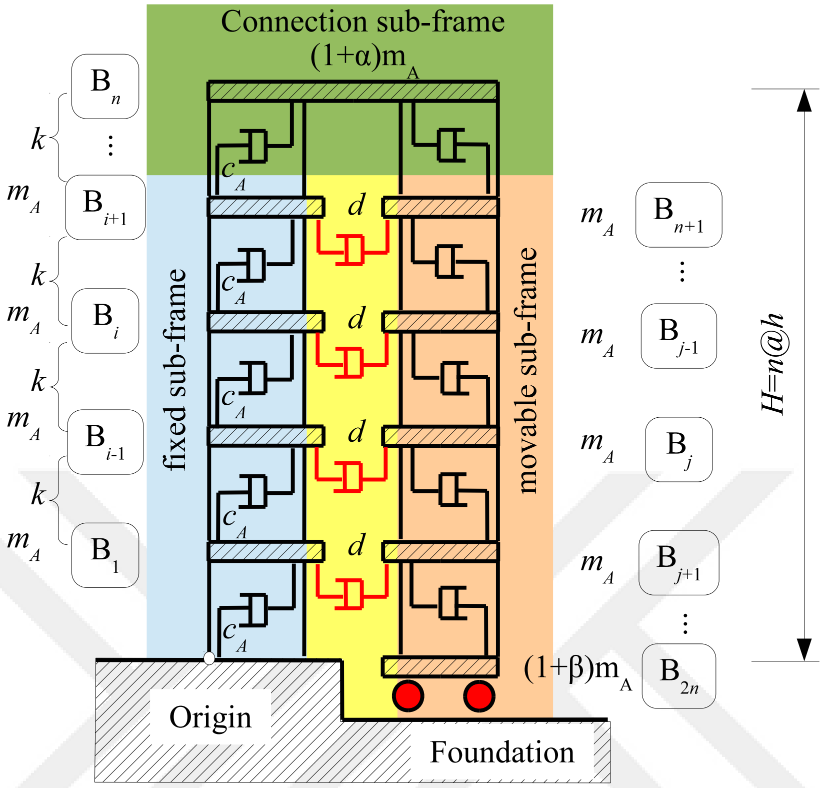

Figure 3.1: Folded cantilever shear structure (System-AD)

of fixed-subframe, and from beam-$(n+1)$ to beam-$(2n-1)$ on the side of movable sub-frame. The masses of beam-n and beam-$2n$ were represented as $(1+\alpha)m_A$ and $(1+\beta)m_A$ where α and β are the mass factors of Bn and $B2n$, respectively. In the following sections, dynamic parameters of the proposed vibration model were obtained for two different cases, $\alpha = \beta = 0$, that is, the mass of all beams are equal to each other, and $\alpha = 1$ and $\beta = 2$. Besides, each storey of idealized vibration model has equal structural damping ratio of dashpot c_A, and shear spring coefficient k_A.

In the following sections, the equations of motion for the proposed model without and with additional dampers are given, and dynamic parameters for two cases were obtained by numerical analyses.

3.2 Folded cantilever shear structure without additional dampers

The proposed vibration model without additional dampers is illustrated in Figure 3.2, and is named as System-A. System-A is identical to System-AD in every respect except additional dampers.

3.2.1 The equation of motion of undamped building under base excitation

The deformed frame and internal forces of System-A due to displacement excitation are illustrated in Figure 3.2 under $z(t)$ time-varying ground motion, where z is the relative displacement of the base from its origin, and x_1, x_2, $\cdots$, x_{2n} are the lateral displacements of beam B_1, B_2, $\cdots$, B_{2n}

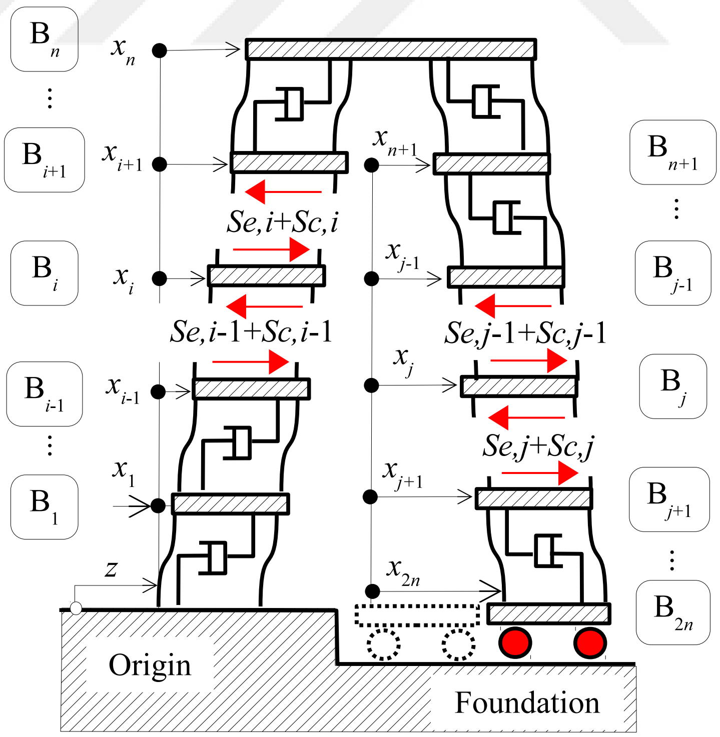

Figure 3.2: Undamped folded cantilever shear structure (System-A)

The relative displacement of the i-th storey of the fixed sub-frame is $z + x_i$ with respect to origin, and shear and viscous damping forces between beam B_i and B_{i+1} are respectively, $S_{e,i}$ and $S_{c,i}$. On the opposite side, the shear and viscous damping forces between beam B_j and B_{j+1} are $S_{e,j}$ and $S_{c,j}$, respectively. The inertia forces of beams are $S_{m,1}$, $S_{m,2}$, $\cdots$, $S_{m,2n}$ for the beam B_1, B_2, $\cdots$, B_{2n}. The equilibriums of the forces on beams B_i, B_j and B_n become;

$$\begin{aligned} -S_{m,i} + S_{c,i} - S_{c,i-1} + S_{e,i} - S_{e,i-1} &= 0 \qquad 1 \leq i < n \\ -S_{m,n} - S_{c,2n-1} - S_{e,2n-1} - fsgn\left(\dot{x}_{2n}\right) &= 0 \end{aligned} \tag{3.1}$$

where, f is the coulomb frictional force resisting against the movement of beam B_{2n}. Besides, $S_{e,i} = k_A(x_{i+1} - x_i)$ and $S_{c,i} = c_A(\dot{x}_{i+1} - \dot{x}_i)$ are the shear and damping forces between the beams, respectively. As for beam B_{2n}, $S_{e,0} = k_A x_{2n}$, $S_{c,0} = c_A \dot{x}_{2n}$ and $S_{m,i} = m_A(\ddot{z} - \ddot{x}_{2n})$ are the shear, damping and inertia forces, respectively. After substituting these equations of the forces into Eq. 3.1 the equation of the motion of System-A becomes as the following equation;

$$M_A^{(2n)}\ddot{x}^{(2n)} + C_A^{(2n)}\dot{x}^{(2n)} + K_A^{(2n)}x^{(2n)} = -\ddot{z}M_A^{(2n)}p^{(2n)} - fe_{2n}^{(2n)}sgn\left(\dot{x}_{2n}^{(2n)}\right) \tag{3.2}$$

Here $e_i^{(2n)}$ is the $2n$ size of unit vector, and $\ddot{x}^{(2n)}$, $\dot{x}^{(2n)}$ and $x^{(2n)}$ are the acceleration, velocity and displacement matrix vectors that of $2n$ number of storey, respectively. $K_A^{(2n)}$, $C_A^{(2n)}$ and $M_A^{(2n)}$ are the stiffness, damping and mass matrices.

$$K_A^{(2n)} = k_A Q^{(2n)} \tag{3.3a}$$

$$C_A^{(2n)} = c_A Q^{(2n)} \tag{3.3b}$$

$$M_A^{(2n)} = m_A Q^{(2n)}(I^{(2n)} + J^{(2n)}) \tag{3.3c}$$

$$J^{(2n)} = \alpha e_n^{(2n)} e_n^{(2n)T} + \beta e_{2n}^{(2n)} e_{2n}^{(2n)T} \tag{3.3d}$$

Here $J^{(2n)}$ is the mass matrix component of B_n and B_{2n} with α and β mass factors of different values, which is $2n$ size of square matrix in condition that all elements are equal to 0.

3.2.2 Natural period characteristics

Dynamic parameters of System-A can be obtained as in the following equations similar to System-O where $\bar{T}_A$, $\bar{\zeta}_A$, and $\bar{\omega}_A$ stands for natural period, circular frequency and damping ratio of inter-story, respectively.

$$\bar{T}_A = \frac{2\pi}{\bar{\omega}_A} = 2\pi\sqrt{\frac{m_A}{k_A}} \tag{3.4a}$$

$$\bar{\zeta}_c = \frac{c_A}{2\sqrt{m_A k_A}} \tag{3.4b}$$

If the coulomb frictional force of roller bearings is neglected, the eigenproblem becomes;

$$\left\{K_A^{(2n)} - \omega_A^2 M_A^{(2n)}\right\} \varphi_A^{(2n)} = 0 \tag{3.5a}$$

$$\left\{Q^{(2n)} - \lambda_A^2 (I^{(2n)} + J^{(2n)})\right\} \varphi_A^{(2n)} = 0 \tag{3.5b}$$

where λ_A is the eigenvalue for System-A.

$$\lambda_{A,i} = \frac{\omega_{A,i}}{\bar{\omega}_A} = \frac{\bar{T}_A}{T_{A,i}} \tag{3.6}$$

Here $\lambda_{A,i}$ is the i-th natural frequency ratio and the corresponding eigenvector $\varphi_A^{(2n)}$ satisfies the orthogonality condition of following equations;

$$\varphi_{A,i}^{(2n)T} Q^{(2n)} \varphi_{A,j}^{(2n)} = \delta_{ij} \lambda_{A,i}^2 \tag{3.7a}$$

$$\varphi_{A,i}^{(2n)T} (I^{(2n)} + J^{(2n)}) \varphi_{A,j}^{(2n)} = \delta_{ij} \tag{3.7b}$$

In condition that the mass factors are equal to each other and zero, α = β = 0, eigenvalues and eigenvectors of System-A can be calculated by using following equations after substituting $2n$ instead n of Eq. 2.9 and Eq. 2.10b,

$$\lambda_{A,i} = 2sin\left(\frac{2i-1}{4 \times 2n + 2}\pi\right) \tag{3.8}$$

$$\varphi_{A,i}^{(2n)} \equiv [\phi_{A,1,i}, \phi_{A,2,i}, \cdots, \phi_{A,2n,i}]^T \tag{3.9a}$$

$$\phi_{A,j,i}^{(n)} = \frac{2}{\sqrt{2 \times 2n + 1}} sin\left(\frac{2i-1}{2 \times 2n + 1} j\pi\right) \tag{3.9b}$$

By proportioning Eq. 3.6 and Eq. 3.8, the ratio between natural period of the vibration model, $T_{A,i}$ and of inter-story, $\bar{T}_A$ can be expressed as follow;

$$\frac{T_{A,i}}{\bar{T}_A} = \frac{1}{2} cosec\left(\frac{2i-1}{4 \times 2n + 2}\pi\right), \qquad 1 \leq i \leq n \tag{3.10}$$

An approximate equation becomes as follows to obtain the first natural period of System-A when $1 \ll n$,

$$T_{A,1} \approx \frac{\bar{T}_A}{\pi}(4n+1) \tag{3.11}$$

It can be estimated that the first natural period of vibration model is extended by increasing the number of storey n, for a given inter-story period $\bar{T}$, which can be calculated by means of specified mass and spring coefficient value, by comparing the Eq. 2.12a and Eq. 3.11.

The natural period of the System-A is almost two times than of System-O, Eq. 3.12 as long as the inter-story periods are same of System-A and System-O.

$$\frac{T_{A,1}}{T_1} \approx \frac{\bar{T}_A}{\bar{T}} \times \frac{4n+1}{2n+1} \approx 2\frac{\bar{T}_A}{\bar{T}} \tag{3.12}$$

3.2.3 Natural vibration mode characteristics

Figure 3.3 presents the relation of System-O and System-A between the natural periods, the first, second and third natural periods, and the number of storey n, obtained by using Eq. 2.6b, Eq. 3.5b and Eq. 3.12.

The relation of the natural period and number of storey of System-A was presented in two conditions; (i) $\alpha = \beta = 0$, that is, all masses are equal for each floor, (ii) $\alpha = 2$, $\beta = 1$ that is, the mass of beam-n is three times and the mass of beam-$2n$ two times of floor masses. The

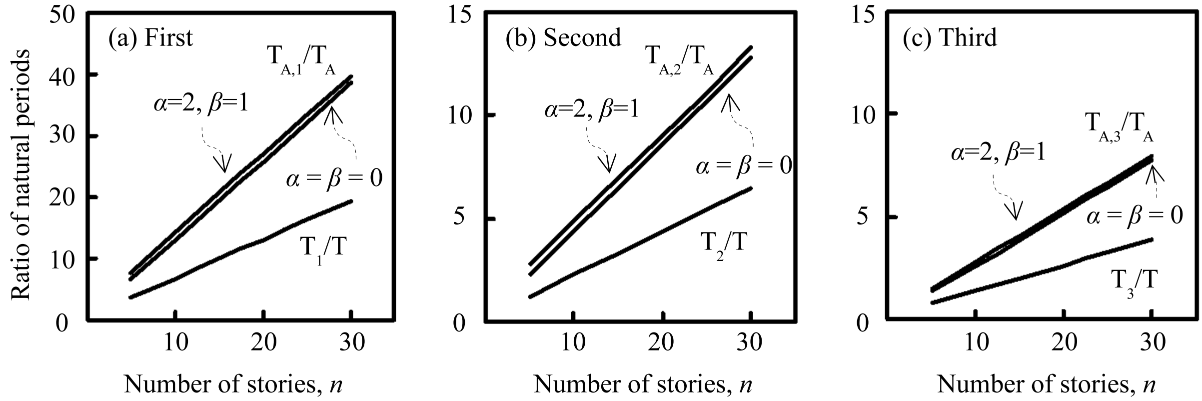

Figure 3.3: Natural period - storey number relation between System-O and System-A

natural period of the former condition is calculated by using Eq. 3.12 and the latter condition by using eigenvalue λ_A obtained from the numerical solution of Eq. 3.5b. In Figure 3.3 the natural period of the System-A is obtained around two times longer than of System-O. As for mass difference in condition that $\alpha = 2$, $\beta = 1$ the difference is quite small in terms of natural periods. As expected, natural periods are increased as long as the number of story increases.

Figure 3.4 presents the first, second, third and fourth natural vibration modes of System-A obtained by using Eq. 3.9b on condition that, $\alpha = \beta = 0$, $n = 10$. To make it easy to understand, the floors of the fixed sub-frame are represented by black dots, • whereas the movable sub-frame floors are represented by white dots, ◦. The natural vibration mode shapes are plotted for the first four modes.

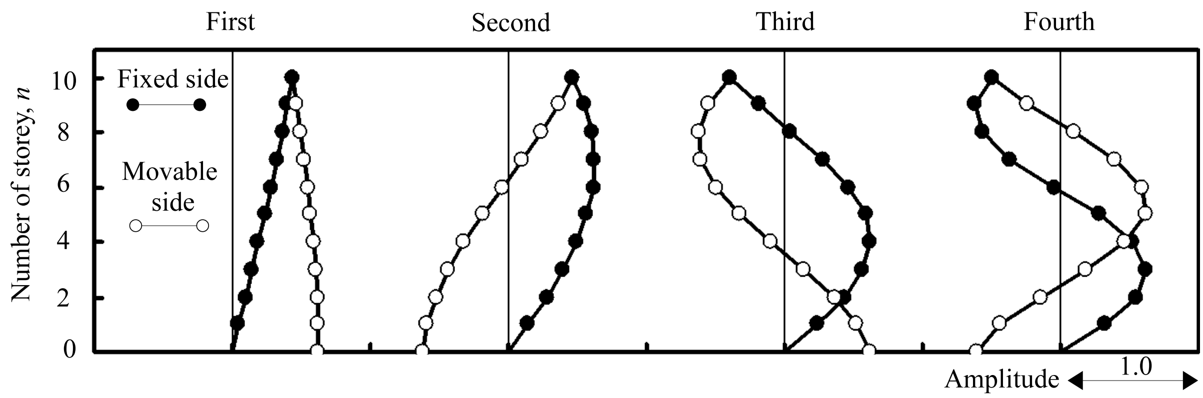

Figure 3.4: Natural vibration modes of System-A ($\alpha = \beta = 0, \quad n = 10$)

3.2.4 Viscous damping characteristics

The proportion of viscous damping ratios of the vibration model $\zeta_{c,i}$, and of inter-storey $\bar{\zeta}_c$ becomes;

$$\frac{\zeta_{c,i}}{\bar{\zeta}_c} = \lambda_{A,i} \tag{3.13a}$$

by using the eigenvector $\varphi_{A,i}^{(2n)}$ and viscous damping ratio of System-A, due to orthogonality condition of Eq. 3.7a and Eq. 3.7b. Taking the mass factors as $\alpha = \beta = 0$ in Eq. 3.8 let us obtain the proportional damping ratios;

$$\frac{\zeta_{c,i}}{\bar{\zeta}_c} = 2sin\left(\frac{2i-1}{4\times 2n+2}\pi\right) \tag{3.13b}$$

The approximate equation of the first natural damping constant can be estimated on the basis of the Eq. 3.13b on condition that $1 \ll n$;

$$\zeta_{c,1} \approx \frac{\pi\bar{\zeta}_c}{4n+1} \tag{3.14}$$

It is seen that, the storey number n, and viscous damping constant $\zeta_{c,1}$ due to dashpots c_A have an inverse proportion as long as $\bar{\zeta}_c$ is specified. Proportioning the Eq. 2.15a and Eq. 3.14 gives us the first viscous damping ratio equation of System-O and System-A.

$$\frac{\zeta_{c,1}}{\zeta_1} \approx \frac{\bar{\zeta}_c}{\bar{\zeta}} \times \frac{2n+1}{4n+1} \approx \frac{1}{2} \times \frac{\bar{\zeta}_c}{\bar{\zeta}} \tag{3.15}$$

The viscous damping ratio of System-A becomes $1/2$ of System-O for the same value of damping constant. Figure 3.5 presents the relation between damping constant and number of storey n, for the first, second and third vibration modes, obtained by using Eq. 2.14 and Eq. 3.13b. The mass factor conditions, α and β of System-A is identical to conditions of Figure 3.3. Damping ratio of System-A is obtained $1/2$ of System-O for the same viscous damping constant value. Besides, the viscous damping constant of System-A, on condition that $\alpha = 2$, $\beta = 1$, for differs a little in contrast in condition that $\alpha = \beta = 0$ for $n \leq 10$. But if the storey number increases, especially for $n > 10$, the difference becomes smaller.

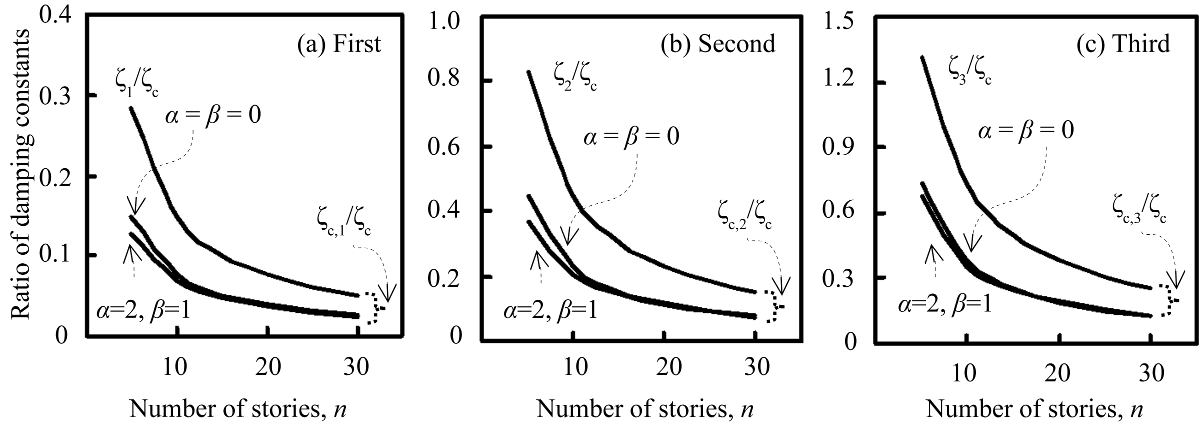

Figure 3.5: Damping constant - storey number relation between System-O and System-A

3.3 Folded cantilever shear structure with additional dampers

As mentioned before, it is possible to increase natural period by increasing flexibility of the structure but this causes extreme displacements. Therefore, additional viscous dampers attached between the beams of sub-frames in the horizontal direction at each floor to reduce inter-story drifts and to increase damping ratio as well. System-A, is investigated again with supplemental dampers, and the new system called from hereafter as System-AD.

3.3.1 The equation of motion of damped building under base excitation

The deformed frame and internal forces of System-AD due to base excitation are illustrated on Figure 3.6

The additional viscous damper opposing beam B_i and B_{2n-i} is removed and replaced by the $P_{i,2n-i}$ vectors of viscous damping force. The equilibriums of the forces for these opposite beams, B_i and B_{2n-i} become;

$$\begin{aligned} &-S_{m,i} + S_{c,i} - S_{c,i-1} + S_{e,i} - S_{e,i-1} + P_{i,j} = 0 && 1 \leq i < n \\ &-S_{m,j} + S_{c,j} - S_{c,j-1} + S_{e,j} - S_{e,j-1} - P_{i,j} = 0 && 1 \leq i \leq n-1 \quad j = 2n-1 \end{aligned} \tag{3.16}$$

and the equilibrium of the forces for beam B_n and B_{2n} becomes;

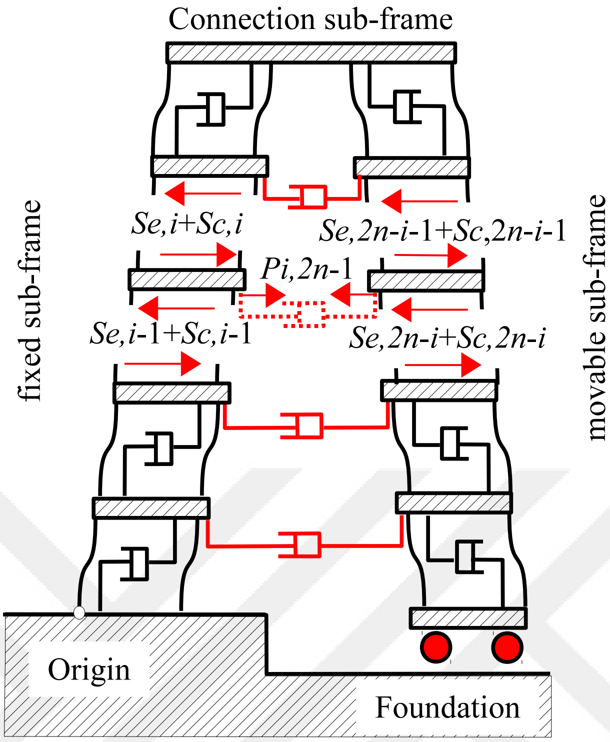

Figure 3.6: Damped folded cantilever shear structure (System-AD)

$$\begin{aligned} -S_{m,n} + S_{c,n} - S_{c,n-1} + S_{e,n} - S_{e,n-1} = 0 \\ -S_{m,2n} - S_{c,2n-1} - S_{e,2n-1} - P_{0,2n} = 0 \end{aligned} \tag{3.17}$$

where, the viscous damping forces are $P_{i,2n-1} = d(\dot{x}_{2n-1} - \dot{x}_i)$ and $P_{0,2n} = d(\dot{x}_{2n})$ By substituting these equations of the forces into the Eq. 3.16 and Eq. 3.17 the equation of the motion of System-AD becomes;

$$M_A^{(2n)}\ddot{x}^{(2n)} + (C_A^{(2n)} + D^{(2n)})\dot{x}^{(2n)} + K_A^{(2n)}x^{(2n)} = -\ddot{z}M_A^{(2n)}p^{(2n)} - fe_{2n}^{(2n)}sgn\left(\dot{x}_{2n}^{(2n)}\right) \tag{3.18}$$

here, $D^{(2n)}$ is the damping matrix of the viscous damper d,

$$D^{(2n)} = dD_0^{(2n)} \tag{3.19a}$$

$$D_0^{(2n)} = e_{2n}^{(2n)}e_{2n}^{(2n)T} + \sum \left[e_i^{(2n)}, e_{2n-i}^{(2n)}\right] \begin{bmatrix} 1 & -1 \\ -1 & 1 \end{bmatrix} \left[e_i^{(2n)}, e_{2n-i}^{(2n)}\right]^T \tag{3.19b}$$

3.3.2 Complex eigenvalue analysis

System-AD becomes non-proportional damping vibration system due to sequence characteristics of matrix $D_0^{(2n)}$ of Eq. 3.19b, and eigenvector $\varphi_{A,i}^{(2n)}$ cannot diagonalize the damping matrix $C_A^{(2n)} + D^{(2n)}$. Therefore, viscous damping ratio and complex eigenvalues of the non-proportional damping vibration system are obtained by using Foss Method [16]. If the coulomb friction force of roller bearings and damping matrix $C_A^{(2n)}$ of System-AD are neglected, the eigenproblem of the additional damped system becomes;

$$\left\{\tau^2 M_A^{(2n)} + \tau D_0^{(2n)} + K_A^{(2n)}\right\} \Psi = 0 \tag{3.20a}$$

where τ and Ψ are complex eigenfrequency and complex eigenvector of System-AD, respectively. When the matrices, $Q^{(2n)}$, $R^{(2n)}$ and $D_0^{(2n)}$, are substituted in Eq. 3.20a the equation becomes;

$$\left\{\sigma^2 (I^{(2n)} + J^{(2n)}) + 2\sigma\bar{\zeta}_d D^{(2n)} + Q^{(2n)}\right\} \Psi = 0 \tag{3.20b}$$

here, σ and $\bar{\zeta}_d$ are the complex eigenvalue and damping ratio, respectively.

$$\sigma = \frac{\tau}{\bar{\omega}_A} \tag{3.21}$$

$$\bar{\zeta}_d = \frac{d}{2\sqrt{m_A k_A}} \tag{3.22}$$

Natural period $T_{d,i}$ and natural frequency $\omega_{d,i}$ of the i-th eigenvector of System-AD can be estimated as in follows;

$$\frac{T_{d,i}}{\bar{T}_A} = \frac{\bar{\omega_A}}{\omega_{d,i}} = \frac{1}{|\sigma_i|} \tag{3.23}$$

and the natural period and the natural frequency equations of System-AD becomes with additional dampers, d;

$$\frac{T_{d,i}}{\bar{T}_{A,i}} = \frac{\bar{\omega}_{A,i}}{\omega_{d,i}} = \frac{\lambda_{A,i}}{|\sigma_i|} \tag{3.24}$$

and the viscous damping ratio $\zeta_{d,i}$ of the i-th eigenvector due to viscous damper supplementation can be calculated by the following equation

$$\zeta_{d,i} = \frac{-Re(\sigma_i)}{|\sigma_i|} \tag{3.25}$$

Damping constant alterations of horizontally attached additional viscous dampers and vertically attached dashpots are illustrated in Figure 3.7 obtained by Eq. 3.25 and Eq. 3.13b on condition that $\alpha = \beta = 0$. Viscous damping constants of dashpots $\bar{\zeta}_c$, and additional viscous dampers $\bar{\zeta}_d$ are specified as 0.3 and 0.01, respectively.

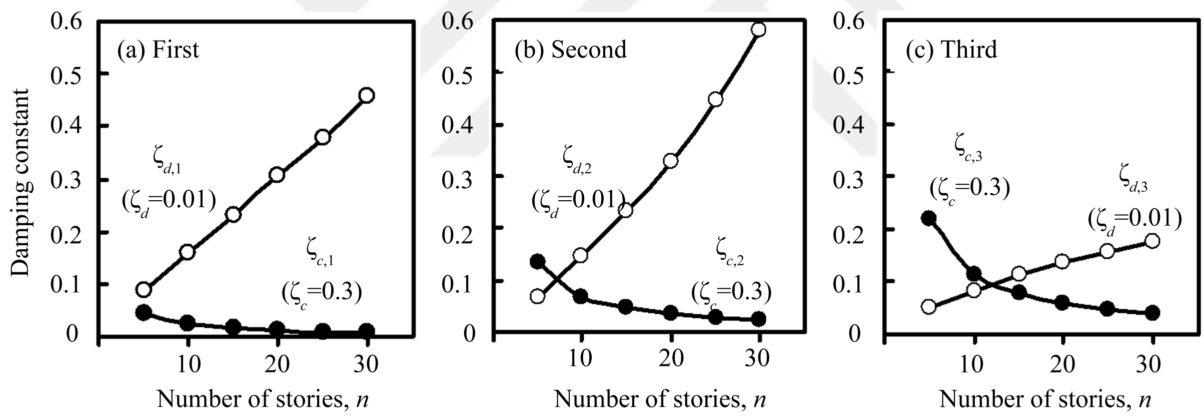

Figure 3.7: Comparison of damping constant of additional viscous dampers and dashpots

By taking the first viscous damping constant of dashpot c_A as 0.02 for the $n = 10$ storey structure, the viscous damping ratio of additional dampers become around 0.26 from Eq. 3.14. In Figure 3.7, the first natural vibration mode shows that the damping constant of horizontal dampers is increased in proportion to number of storey n, whereas the damping constant of dashpots is decreased. In spite of similar damping constant for $n = 6$ number of storey, the damping constant alteration becomes remarkable, up to 30 times, as long as the number of storey increases.

Figure 3.8 illustrates alteration of natural periods of first, second and third modes obtained using Eq. 3.24 due to additional viscous dampers. Calculation parameters are same with those

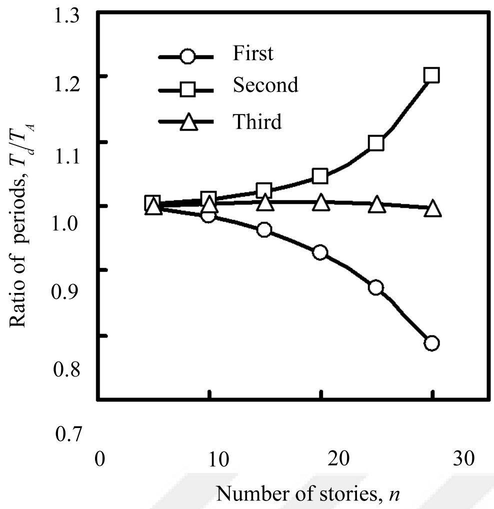

Figure 3.8: Alteration of natural periods due to additional viscous dampers

of Figure 3.7 except $\bar{\zeta}_c$ which was set to 0. The change was remained within 2% for the first mode of natural period and 1% for the second mode of natural period. The alteration for third mode of natural period was obtained very small. The horizontal placement of additional dampers was obtained more effective than of vertically attached dashpots. Besides, the natural period of first mode alteration was remained almost same due to additional dampers. Therefore the proposed structure, System-AD, let us to extend the natural period of ordinary structure 2 times by increasing floor number and attaching additional dampers between opposing beams of sub-frames. Finally, the corresponding viscous damping ratio of the i-th natural frequency of System-AD can be obtained by substituting the damping matrix $C_A^{(2n)}$ of additional dampers into Eq. 3.20a, the viscous damping ratio of System-A,

$$\bar{\zeta}_{AD,i} \approx \bar{\zeta}_{A,i} + \bar{\zeta}_{d,i} = \bar{\zeta}_{c,i} + \bar{\zeta}_{f,i} + \bar{\zeta}_{d,i} \tag{3.26}$$

3.4 Conclusion

In this chapter, the dynamic characteristics of the proposed folded cantilever shear structure is introduced. Similar to the ordinary building equations, some simple equations are derivated for the proposed vibration model. Natural vibration mode characteristics, viscous damping characteristics are investigated for proposed building with and without additional dampers.

CHAPTER 4

Numerical Studies of Folded Cantilever Shear Structure

4.1 Introduction

To examine the theory of proposed structure, a set of numerical analyses including eigenvalue and elastic dynamic response analyses were performed through three idealized models, OCSS, System-O, and FCSS without and with additional dampers, System-A and System-AD, respectively. System-O is the comparison model for FCSS models. Besides, it is aimed to examine behavioral differences between FCSS without and with additional damper systems. Table1 summarizes the structural model parameters of spring-mass models of numerical analyses. All models are 15-storey with 50 m of height (each storey height is 3.33 m).

The given parameters are not consistent and were specified due to a chart presenting the observed natural periods of steel and reinforcement concrete buildings of mid-rise buildings around Japan. Natural period of 50 m building was assumed around 1 sec, then specifying mass of floor let us estimated shear spring coefficients for ordinary buildings. As for System-O, columns are modelled as spring elements with 3.85×10^8 Nm of shear spring coefficient, which was represented as k_1, k_2, $\cdots$, k_{14} and k_{15}. The storey masses which were concentrated at the beams represented as m_1, m_2, $\cdots$, m_{14} and m_{15} and each of them were equalled to $100,000$ kg that makes the total mass $1,500,000$ kg. Damping coefficients of the dashpots, c_1, c_2, $\cdots$, c_{14} and c_{15}, were set to 2.5×10^6 Ns/m.

FCSS models have the same height with OCSS model. The concentrated masses of the fixed shear sub-frame and movable shear sub-frames were represented as k_1, k_2, $\cdots$, k_{14} and k_{16}, k_{17}, $\cdots$, k_{29}, k_{30}, respectively. The mass of each beam at the fixed and movable sides were,

Table 4.1: Spring-mass model parameters

Parameter	FCSS - System AD	OCSS - System O
Total height, H	$50m$	$50m$
Number of stories, n	15	15
Storey height, h	$3.33m$	$3.33m$
Storey mass	$m_1 \sim m_{14} = 50,000kg$	$m_1 \sim m_{30} = 100,000kg$
Total mass, m	$1,600,000kg$	$1,500,000kg$
Shear spring coefficient	$k_1 \sim k_{30} = 1.60 \times 10^8 Nm$	$k_1 \sim k_{15}$ = $3.85 \times 10^8 Nm$
Structural damping coefficient	$c_1 \sim c_{30}$ = $1.11 \times 10^6 Ns/m$	$c_1 \sim c_{15}$ = $2.50 \times 10^6 Ns/m$
First structural damping ratio	$\zeta_1 = 1\%$	$\zeta_1 = 2\%$
Additional damping coefficient	$d_0 \sim d_{14} = 0.25 \times 10^6 Ns/m$	–
First additional damping ratio	$\Delta\zeta_1 = 34\%$	–
Frictional coefficient	$\mu = 0.005$	–
Frictional force, N	$f = 41,650N$	–

$m_1 \sim m_{14}$ and $m_{16} \sim m_{30}$, $50,000$ kg. However the rigid connection beam, m_{15} was $100,000$ kg. The total mass of the FCSS models became $1,550,000$ kg. The shear spring coefficients, $k_1 \sim k_{15}$ and $k_{16} \sim k_{30}$, and the damping coefficients, $c_1 \sim c_{14}$ and $c_{16} \sim c_{30}$, were set to 1.60×10^8 Nm and $1,11 \times 10^6$ Ns/m, respectively. Structural damping ratio was also taken 1% for the System-A. System-AD is identical to System-A in terms of the structural height, structural damping ratio, masses, $m_1 \sim m_{30}$, the spring coefficients, $k_1 \sim k_{30}$, and the damping coefficients, $c_1 \sim c_{30}$, except the additional viscous dampers with 0.25×10^6 Ns/m damping coefficients represented as $d_0 \sim d_{14}$.

4.2 Eigenvalue analysis

Obtained natural frequencies, damping ratios and complex eigenvalues by using Foss Method for System-O, ordinary structure, and of System-AD, proposed structure, were given in Table 4.2.

Table 4.2: Complex eigenvalues of System-O and System-AD

	OCSS - System O	FCSS - System AD		
	First	First	Second	Third
$T_d(sec)$	$0,99$	$2,1$	$0,80$	$0,48$
ω_d	$6,285$	$2,985$	$7,899$	$13,217$
ζ	$0,02$	$0,35$	$0,358$	$0,249$
λ_R	$-0,128$	$-1,046$	$-2,825$	$-3,285$
λ_I	$\pm 6,284$	$\pm 2,796$	$\pm 7,377$	$\pm 12,082$

The first natural period of ordinary building was obtained around $T_{1,O} = 1.0$ sec, whereas the proposed buildings' were obtained around $T_{1,AD} = 2,10$ sec, by using computer program of C language using Foss method. It is seen that the proposed structure is capable of extending the natural period with its unique design. Considering that the additional dampers have no effect on natural period, the design of proposed model have one other benefit which is increasing efficiency of additional dampers to be added between sub-frames. Since the sub-frames can move toward each other or away from each other, it is an effective way placing damper devices in horizontal direction for increasing damping ratio.

To make comparison eigenvalues between the computational results by using derived equations of Eq. 2.11 and Eq. 3.10 and computer program of C language using Foss method, the natural periods were obtained $T_{1,O} = 0,99$ sec and $T_{1,AD} = 2,19$ sec, respectively for the given parameters of Table 6.2 when derived equations were used. That is, proposed model acquired two times of first natural period compared to ordinary structure, and derived equations gave agreeable results when compared with computer program results.

In addition, although the structural damping coefficient of the System-AD is taken smaller than System-O, the damping ratio was obtained 9% for FCSS without damper and 35% for System-AD, whereas System-O has 2% of damping ratio. Besides, the damping ratio of System-A, which has no additional dampers, was obtained 9%.

In Figure 4.1 and Figure 4.2 the standstill and vibration modes of System-O and System-AD were given, which represent the ordinary and proposed structures of 15 storey.

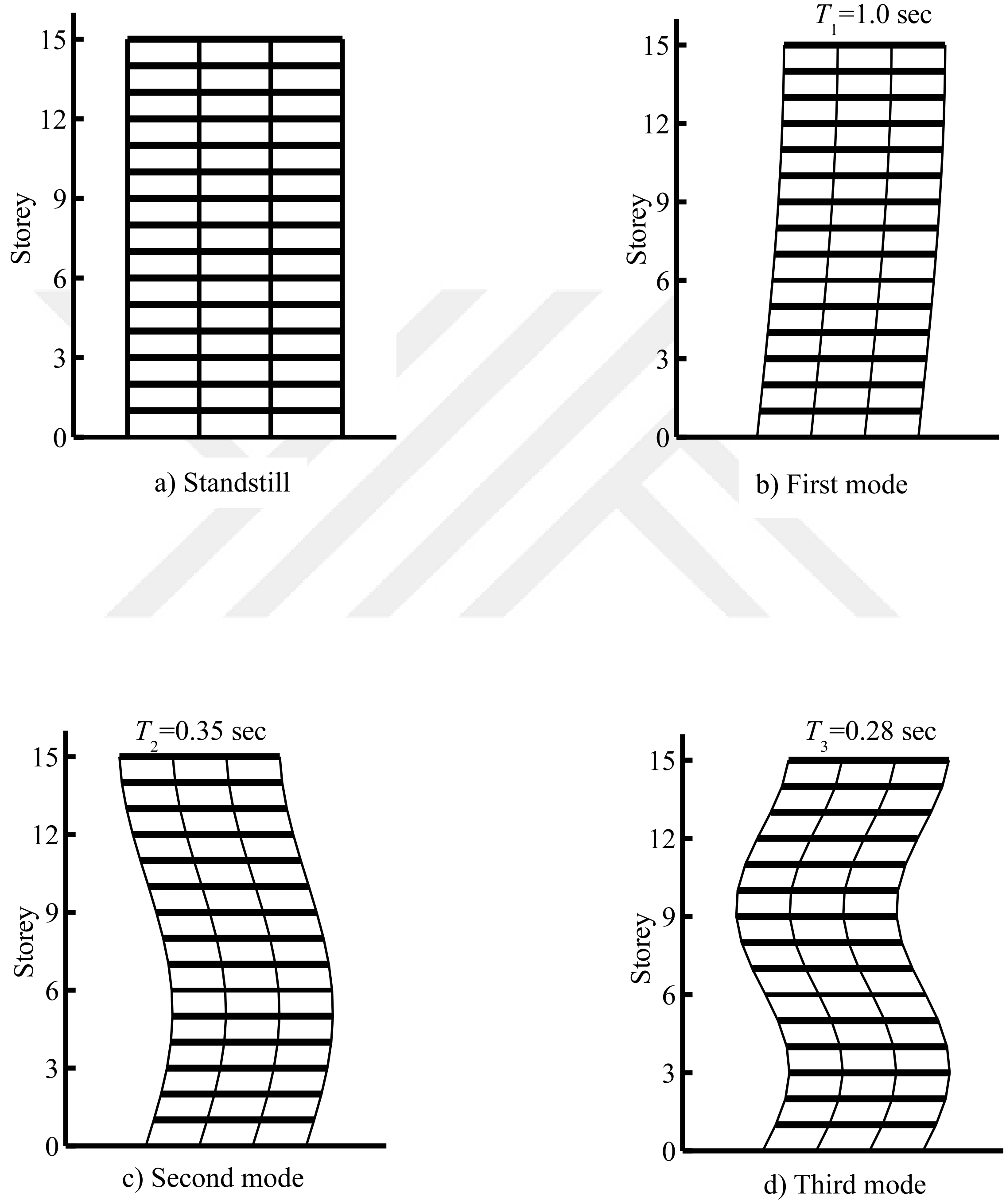

Figure 4.1: Vibration modes of System-O

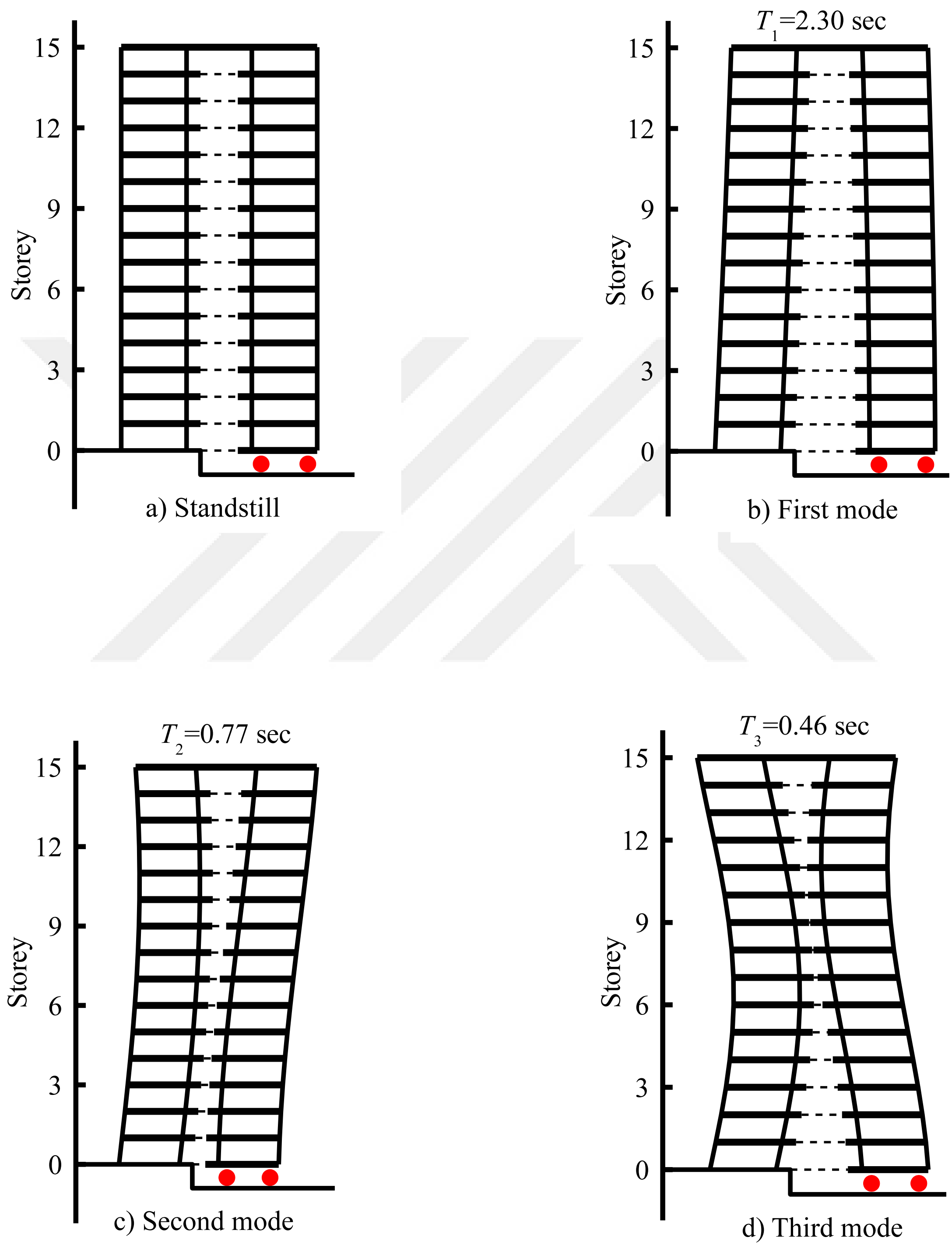

Figure 4.2: Vibration modes of System-AD

4.3 Elastic dynamic response analysis

The elastic dynamic response analysis was conducted to investigate the seismic behaviour of the numerical models, System-O and System-AD, due to El Centro (1940), Taft (1952), Hachinohe (1968) and Miyagi (1978) earthquakes. Those four earthquake waves to be used in computational examples were scaled to 300 gal of maximum acceleration. Then, numerical models with specified parameters, as given in Table 6.2, were subjected to time-history analysis. Figure 4.3 illustrates El Centro earthquake seismic wave, and acceleration and displacement responses of System-O and System-AD.

As for time history results of numerical models, the maximum acceleration response was obtained around 7.7 m/s^2 for ordinary building, and 2.6 m/s^2 for proposed building, System-AD, with additional dampers due to El Centro earthquake wave, Figure 4.3. Relative velocity responses were, 1.4 m/s and 0.4 m/s for System-O and System-AD models, respectively. Finally, relative displacement responses were obtained around 0.18 m and 0.11 m at the roof part of System-O and System-AD, respectively.

As for seismic responses against Taft earthquake wave, Figure 4.5, maximum acceleration were obtained around 6 m/s^2 and 2.7 m/s^2 for System-O and System-AD, respectively. Relative velocity responses were obtained 0.7 m/s and 0.5 m/s and relative displacements were 0.12 m and 0.1 m for System-O and System-AD models, respectively.

Figure 4.7 illustrates the seismic responses against Hachinohe earthquake wave. As it is seen, maximum acceleration responses were obtained around 9.1 m/s^2 and 3.4 m/s^2 for System-O and System-AD models, respectively. Relative velocity responses were 1.4 m/s and 0.3 m/s, whereas the relative displacement responses were obtained 0.15 m 0.22 m for System-O and System-AD, respectively.

As for seismic responses against Miyagi earthquake wave, Figure 4.9 shows that maximum acceleration responses were 18.9 m/s^2 and 3.2 m/s^2 for System-O and System-AD models, respectively. Besides, relative velocity responses were obtained 3 m/s and 0.9 m/s and relative displacements were 0.4 m and 0.11 m for System-O and System-AD models, respectively.

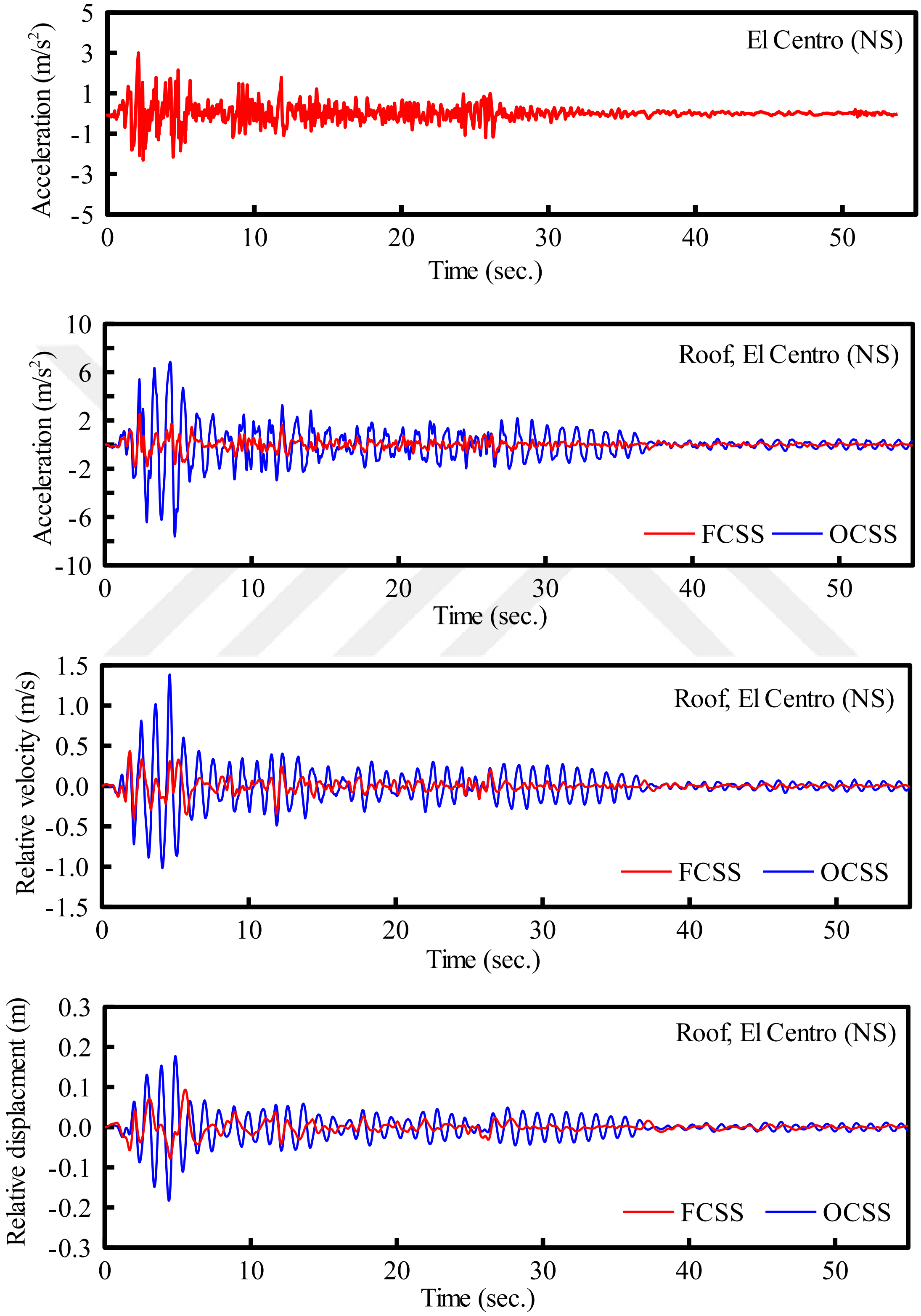

Figure 4.3: El Centro earthquake, responses of System-O and System-AD

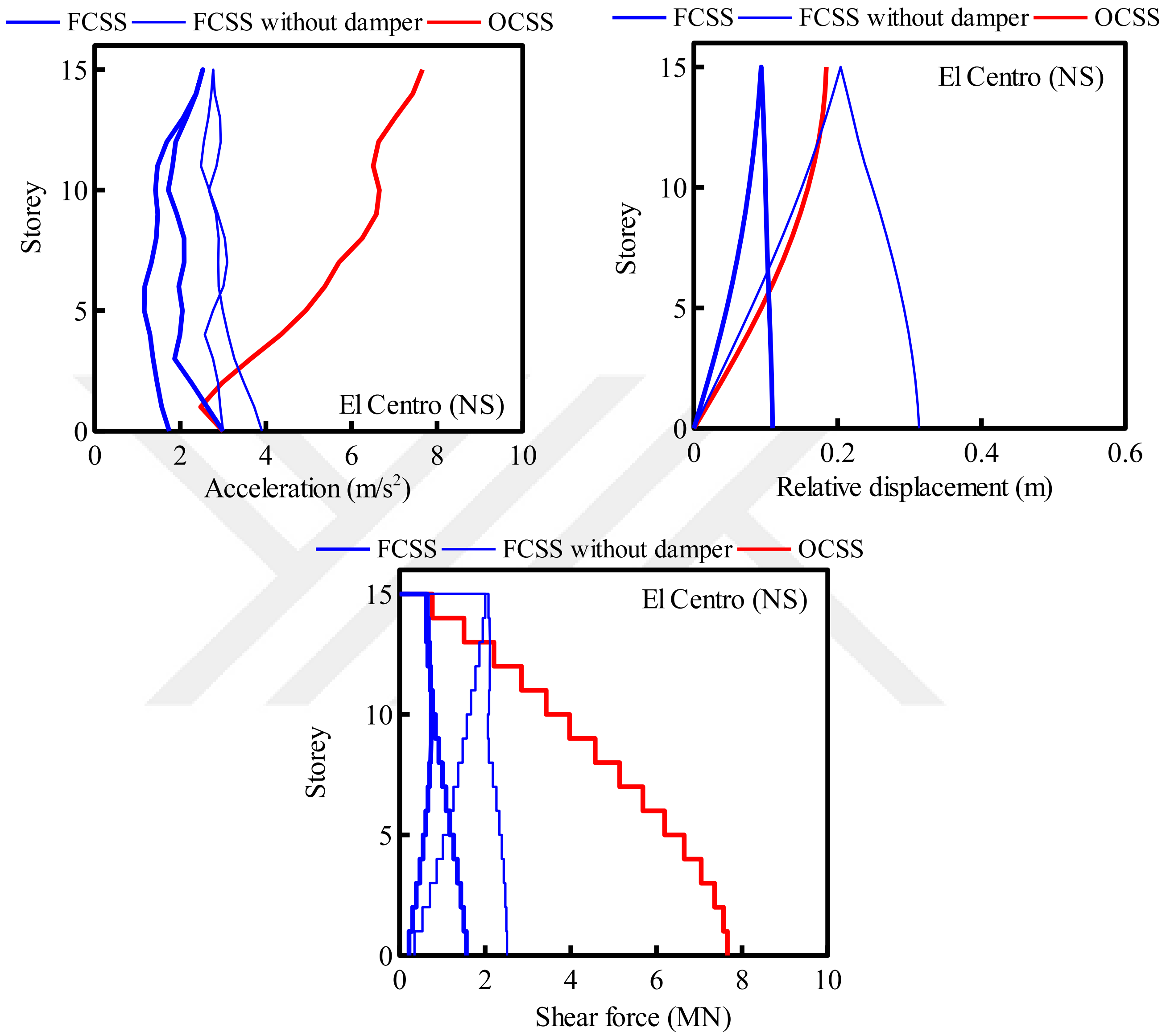

Figure 4.4: Seismic responses due to El Centro earthquake on the base of storey

Figure 4.4 shows the acceleration, relative displacement and shear force responses of System-O, System-A and System-AD due to El Centro earthquake. Figure 4.4 show that maximum acceleration responses were obtained 7.66 m/s^2, 3.91 m/s^2 and 2.57 m/s^2 for System-O, System-A and System-AD, respectively. Relative displacement responses were obtained 0.18 m, 0.31 m and 0.11 m whereas shear force responses were 7.66 MN, 2.51 MN and 1.56 MN at the roof for System-O, System-A and System-AD, respectively.

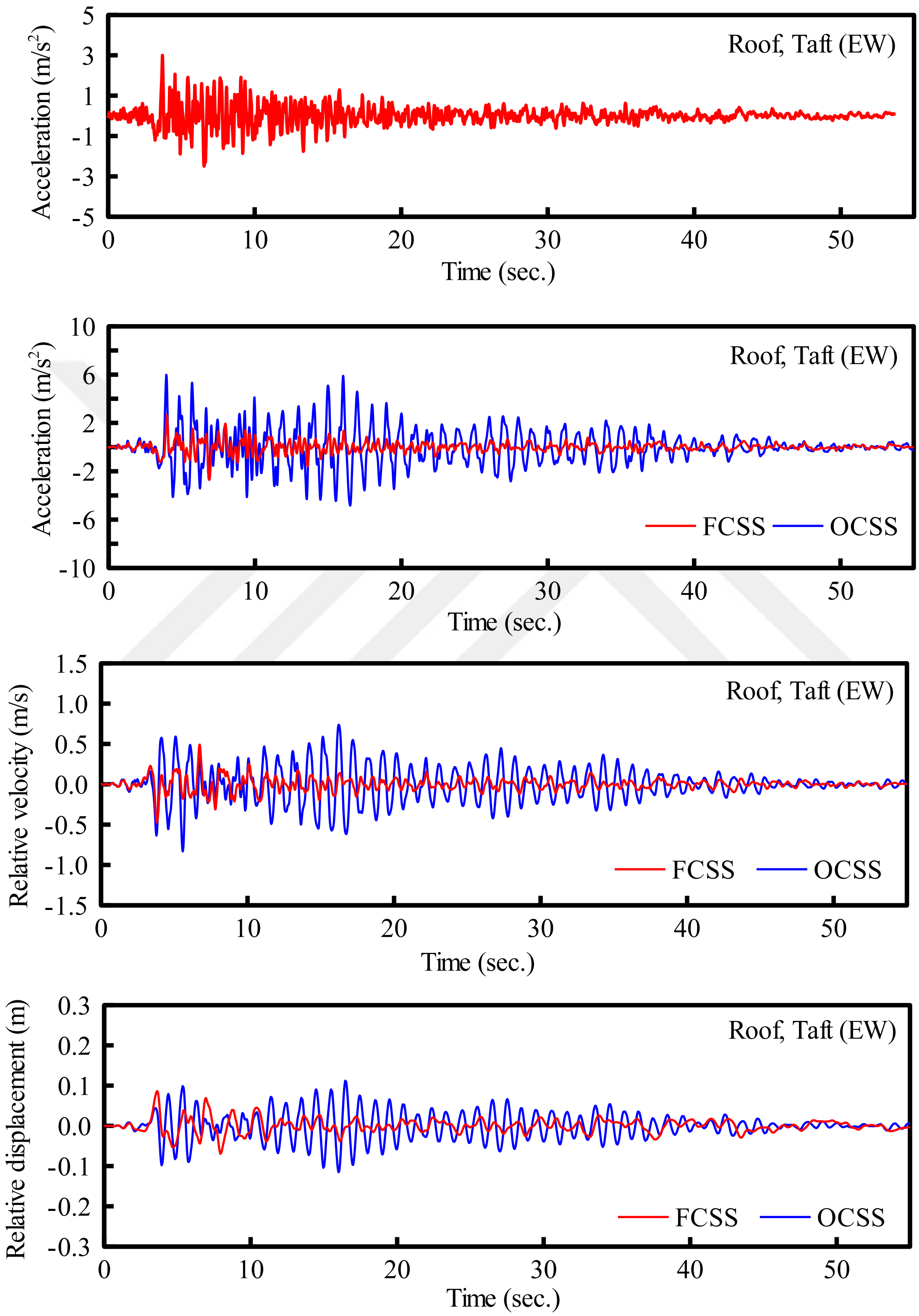

Figure 4.5: Taft earthquake, responses of System-O and System-AD

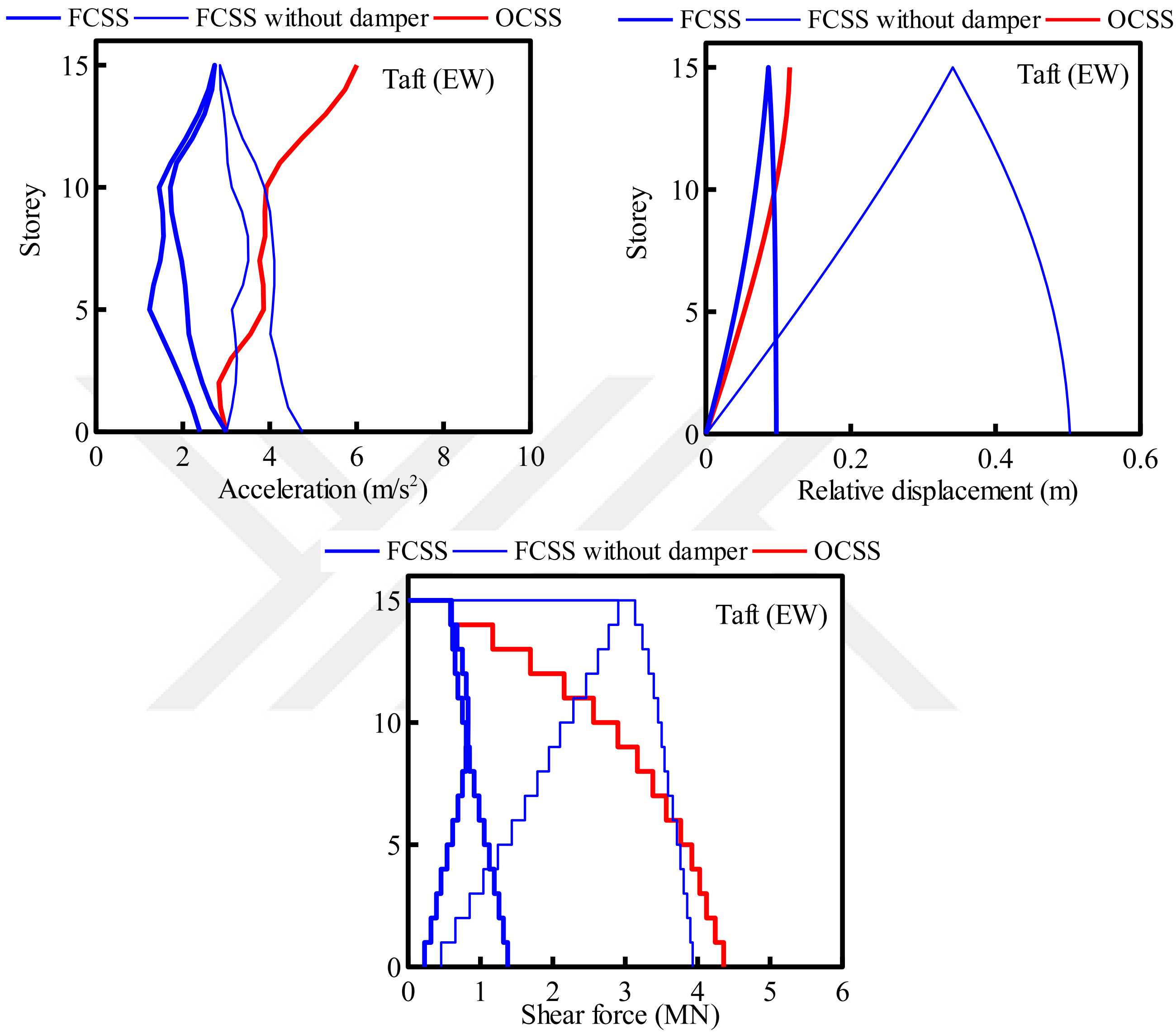

Figure 4.6: Seismic responses due to Taft earthquake on the base of storey

According to the Figure 4.6, maximum acceleration responses were obtained 6.01 m/s^2, 3.96 m/s^2 and 2.73 m/s^2 for System-O, System-A and System-AD, respectively. Relative displacement responses were obtained 0.11 m, 0.19 m and 0.09 m whereas shear force responses were 4.36 MN, 1.97 MN and 1.38 MN at the roof for System-O, System-A and System-AD, respectively.

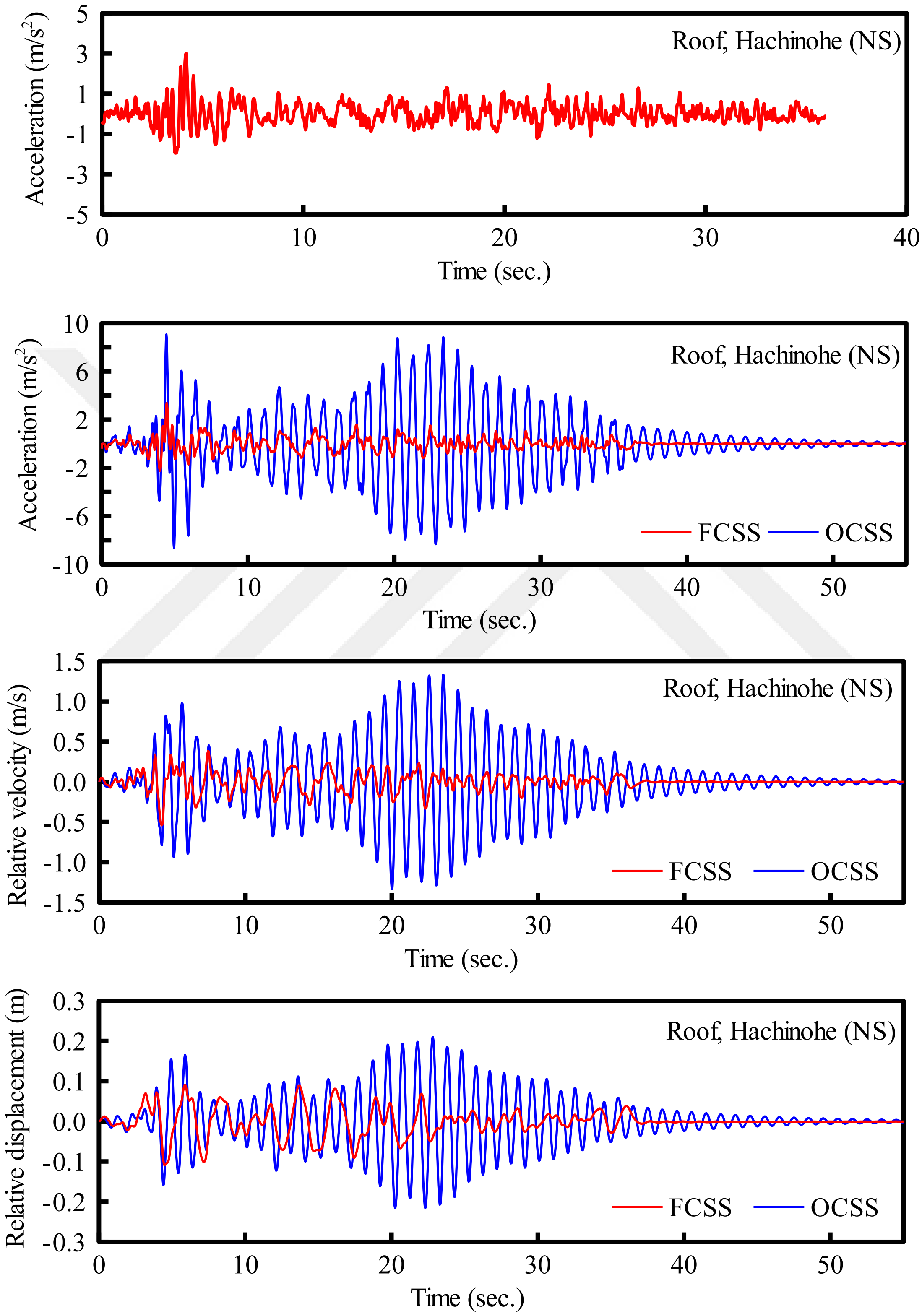

Figure 4.7: Hachinohe earthquake, responses of System-O and System-AD

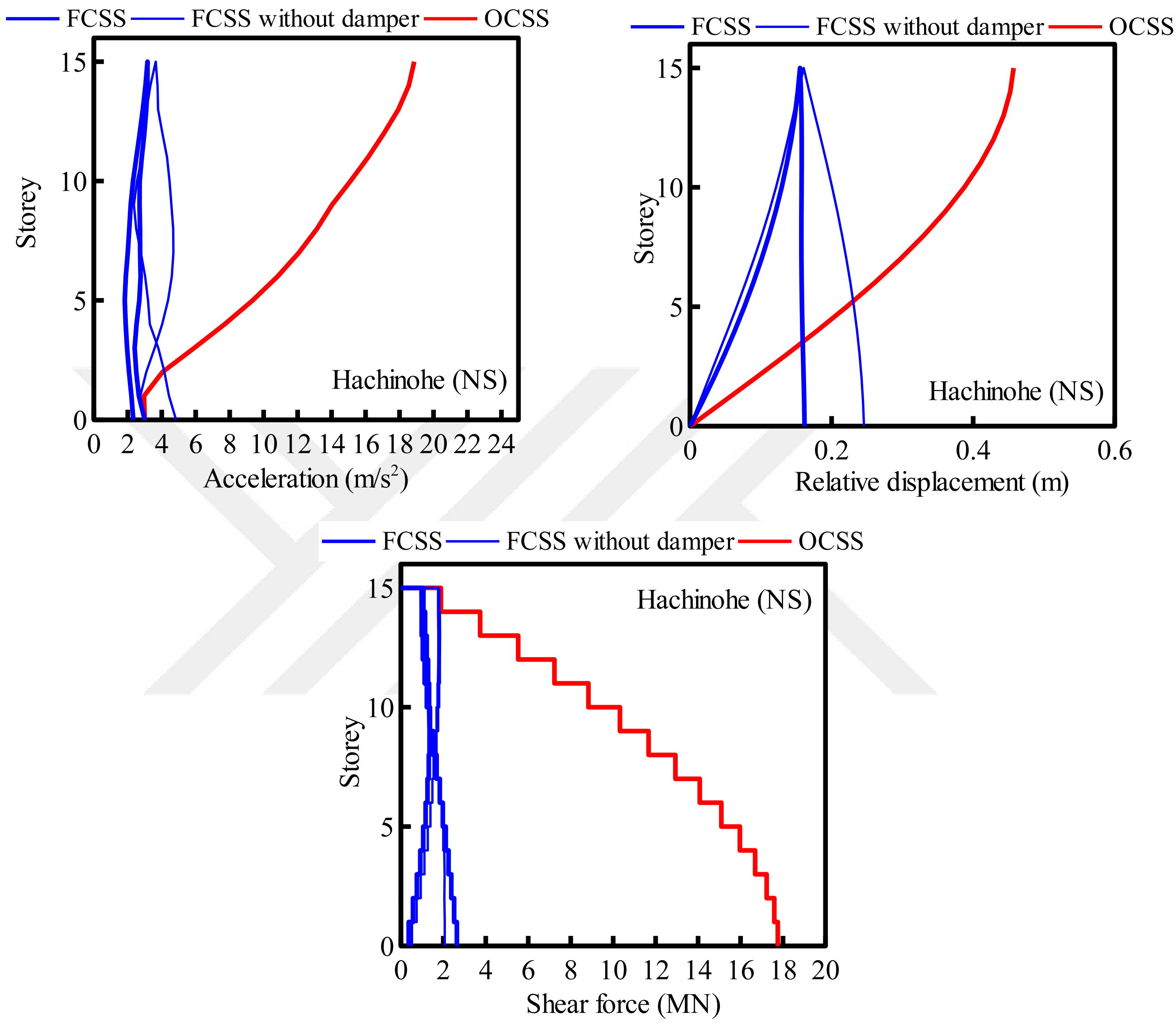

Figure 4.8: Seismic responses due to Hachinohe earthquake on the base of storey

Figure 4.8 shows that, maximum acceleration responses were obtained 9.07 m/s^2, 4.75 m/s^2 and 3.37 m/s^2 for System-O, System-A and System-AD, respectively. Relative displacement responses were obtained 0.21 m, 0.50 m and 0.15 m whereas shear force responses were 8.77 MN, 3.93 MN and 2.04 MN at the roof for System-O, System-A and System-AD, respectively.

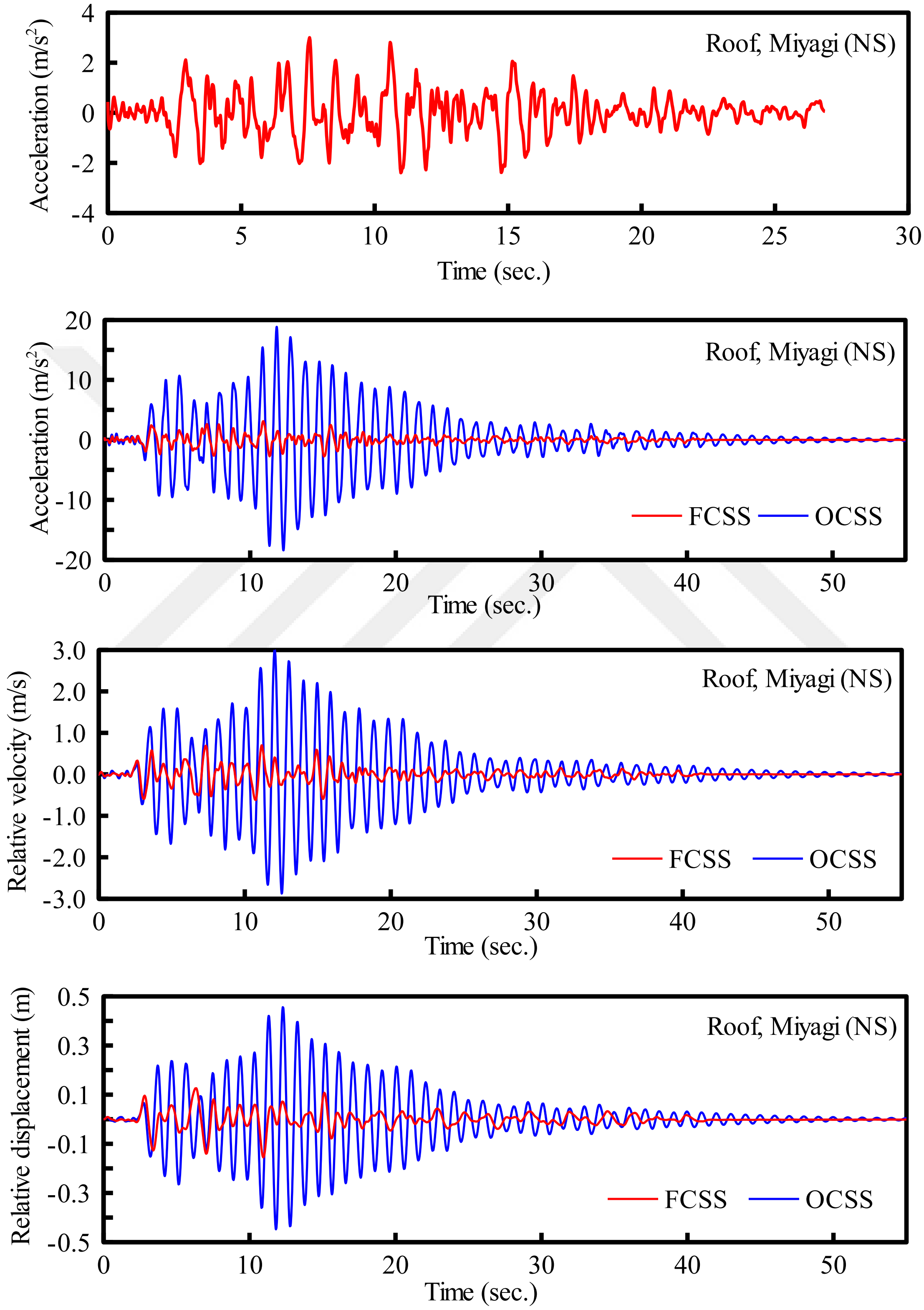

Figure 4.9: Miyagi earthquake, responses of System-O and System-AD

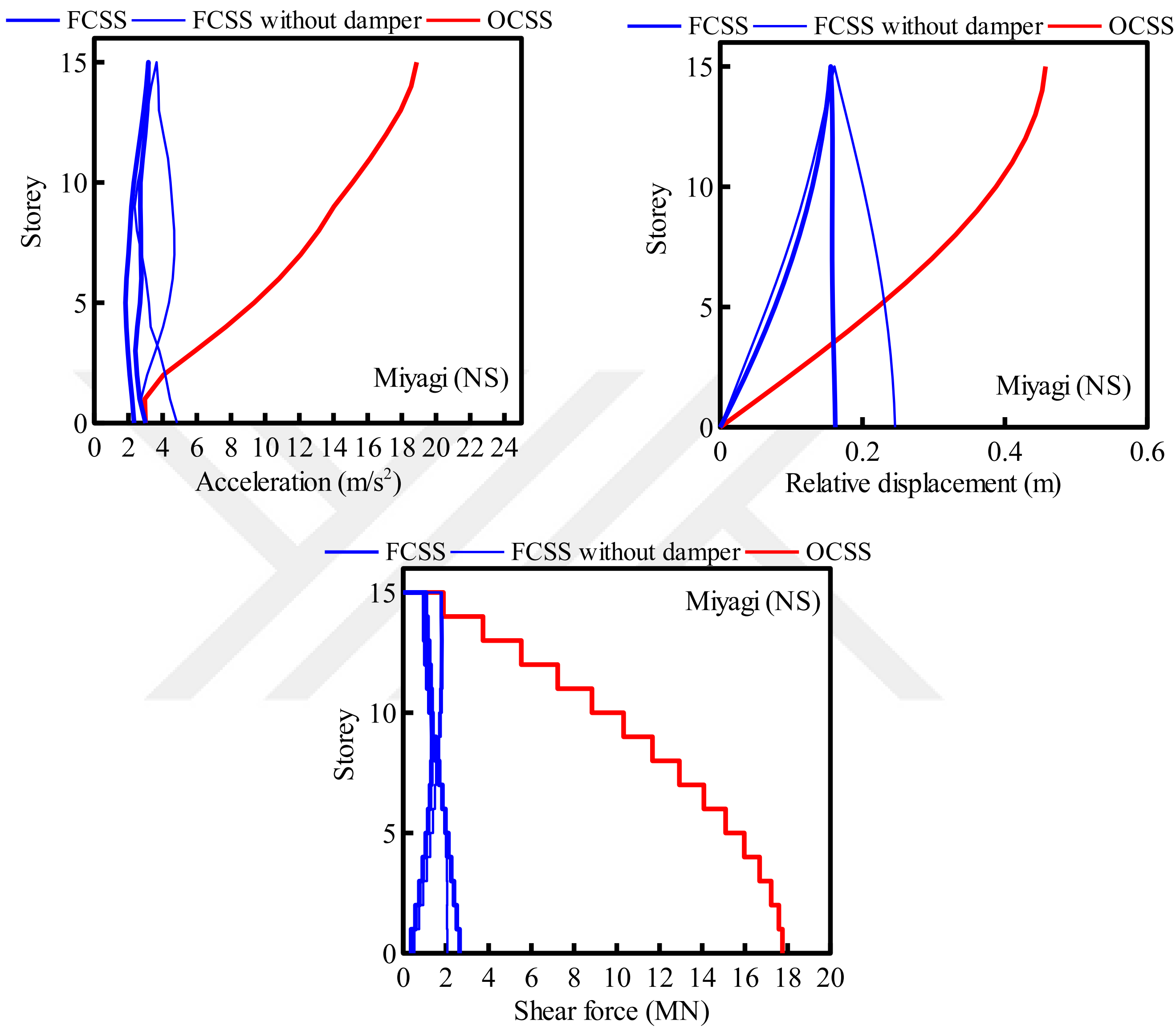

Figure 4.10: Seismic responses due to Miyagi earthquake on the base of storey

According to the Figure 4.10, maximum acceleration responses were obtained 18.87 m/s^2, 4.84 m/s^2 and 3.16 m/s^2 for System-O, System-A and System-AD, respectively. Relative displacement responses were obtained 0.46 m, 0.24 m and 0.16 m whereas shear force responses were 17.75 MN, 2.07 MN and 2.64 MN at the roof for System-O, System-A and System-AD, respectively.

In the following Figure 4.11, all models with their maximum response values are given due to each earthquake wave subjected to numerical models.

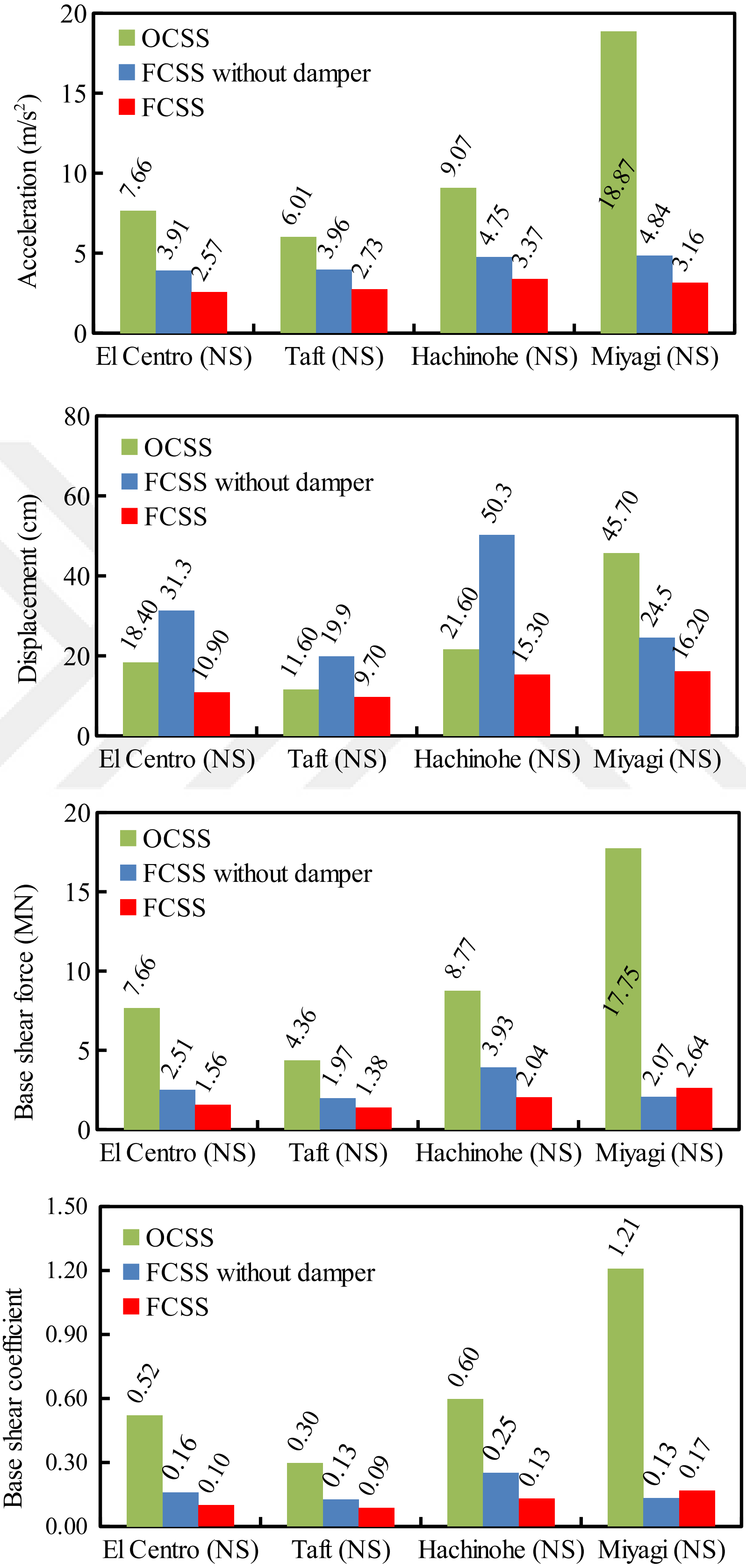

Figure 4.11: Seismic responses due to four earthquake waves for each model

4.4 Conclusion

In this chapter, ordinary building and proposed buildings were modelled as 15-storey high mid-rise buildings and were compared to each other for the specified parameters. These numerical models were subjected to complex eigenvalue analysis and elastic dynamic responses analysis to verify whether the theory of proposed model is correct or not. The theory proposes that using proposed model on condition of same number of storey with ordinary building, the natural period of an ordinary building can be increased by a factor of two.

The results shows that, the acceleration and displacement responses, with respect to base, of ordinary structure reduced up to 69% and 39%, respectively by proposed building. That is, structural responses can be mitigated properly by proposed structure compared to same height of ordinary building. Shear force and acceleration responses were obtained maximum for ordinary building, then System-A and System-AD follows System-O in decreasing response order.

Another point should be noted here is that System-A results also were decreased in terms of acceleration and shear forces but since there is no additional dampers between beams, the relative displacement responses were obtained maximum during seismic movement of numerical model.

CHAPTER 5

Experimental Studies of Folded Cantilever Shear Structure

5.1 Introduction

To examine the theory of proposed structure, a set of numerical analyses including eigenvalue and elastic dynamic response analyses were performed through three idealized models, OCSS, System-O, and FCSS without and with additional dampers, System-A and System-AD, respectively. System-O is the comparison model for FCSS models. Besides, it is aimed to examine behavioral differences between FCSS without and with additional damper systems.

5.2 Experimental model configuration and components

The proposed structure consists of non-isolated and fully-isolated sub-frames of similar heights that are rigidly connected to each other at the top part by using connection sub-frame as in Figure 5.1. That is, three sub-frames are combined in one structure which is able to move along x and y directions on the movable sub-frame side. 16-storey vibration model was constructed by using 230 mm $\times$ 5 mm $\times$ 430 mm and 630 mm $\times$ 5 mm $\times$ 430 mm sized rigid aluminium alloy (A5052) rectangular plates as beams for fixed - movable sub frames and connection sub-frame, respectively. Both sub-frames have 6 circular columns which were made of polycarbonate (PC) screw rods with M10 metric size, and aluminium plates were fixed to the screw rods at each column by tightening one plastic nut down of plate and the other on top of plate. The total height of vibration model was 1470 mm with 90 mm of floor height, Figure 5.1. Columns were set up by fastening two pieces of screw rods which were 1 m and 0.5 m in length. Therefore, the eleventh floor became 120 mm due to additional part of the rod connection. And these rods were fixed to the bottom plate which was 20 mm thick and including holes for mounting the plate on the shaking table.

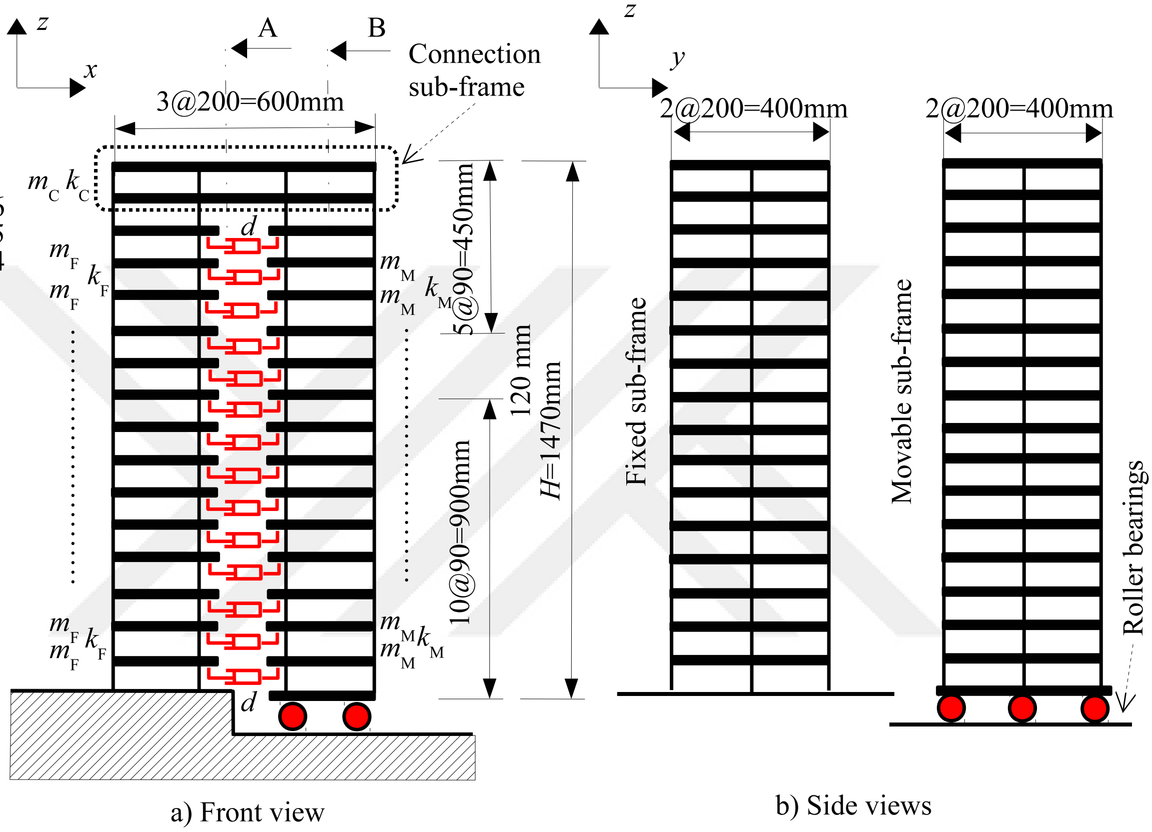

Figure 5.1: Front and cross-sectional side views of experimental vibration model

The clearance between columns was 200 mm along x and y directions. That is, the vibration model was 600 mm in length and 400 mm in width. Fixed sub-frame had an encastre boundary condition at the foundation and movable sub-frame was supported by roller bearings. In order to prevent contact problems between sub-structures during any movement, gaps between dampers after installation to the sub-frames were arranged to be around 30 mm. Dampers of proposed model will be introduced in detail in the following section. According to the tension and bending tests of a polycarbonate rod of column, the axial stiffness (AE) were obtained around 1.10×10^5 N and flexural stiffness (EI) was 5.65×10^5 Nmm^2. In Fig.5.1 m_F, m_M and m_C stands for the floor mass of fixed, movable and connection sub-frames, respectively and k_F, k_M and k_C represents the lateral shear spring coefficients as well. The total mass of floors including beam, column and viscous damper device masses were arranged to be 3 kg for each side after installation of additional masses which were tightened to the plates at the mid-point. And total mass of connection floors and movable bottom floor were arranged to be 4.5 kg and 3.5 kg, respectively. The lateral shear coefficient tests of the columns were discussed in the following section.

5.2.1 Lateral stiffness coefficient investigation of polycarbonate columns

a) Experimental test model

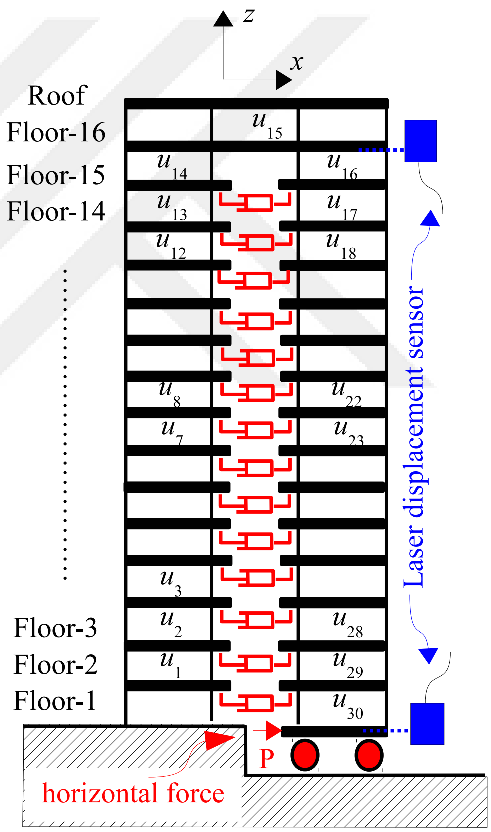

b) Quasi-static load test subjecting lateral force

Figure 5.2: Lateral stiffness coefficient investigation models

Lateral shear spring coefficients of inter-storey columns, k_F and k_M of fixed and movable sub-frames, were investigated by conducting quasi-static loading test on the vibration test model, Figure 5.2.

The movable bottom floor was subjected to the lateral force of P, and the displacement of movable bottom floor, u_{30} and the top floor of connection sub-frame, Floor-16, u_{15} were obtained by using laser displacement sensors as illustrated in Figure 5.2.b. Besides, u_1, u_2, u_3, $\cdots$, u_{14} and u_{16}, u_{17}, u_{18}, $\cdots$, u_{29} represents the lateral displacements of each floors along x direction.

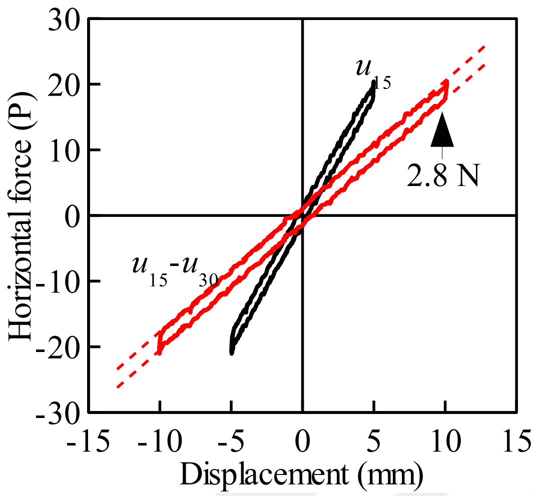

Figure 5.3: Quasi-static loading test results

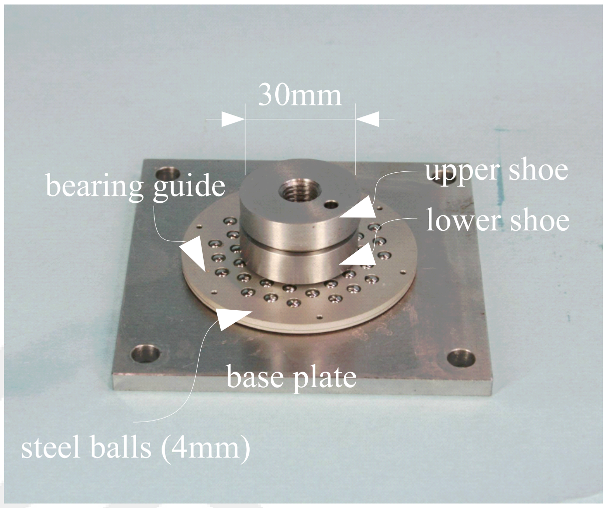

Figure 5.4: Roller bearing device

According to the quasi-static lading test results, the lateral force - displacement history curves were obtained as in Figure 5.3 for floor-16 u_{15}, and for movable bottom floor u_{15-30}. The slope of history curve at Floor-16 was around 0.00382 N/m and estimated stiffness coefficient became 57.3 kN/m. As for movable bottom floor, the stiffness coefficient was obtained around 57.0 kN/m. The stiffness of columns to be used in simulations, eigenvalue analysis and elastic dynamic response analysis, was taken as the average of these obtained two values that was equal to 57.15 kN/m. And the force gap due to loading - unloading between parallel lines of history curve was obtained around 2.8 N, Figure 5.3.

Roller bearing, designed and tested in the Structural Dynamics Laboratory of Sojo University, was chosen as the base isolation unit for the proposed structure. And the test mechanism to examine the friction coefficient curve of roller bearing device is elaborated in the following section.

5.2.2 Roller bearing device

Roller bearing device components consist of 30 mm diameter of upper and lower shoes, 60 mm diameter of bearing guide and 6 mm thickness of base plate, Figure 5.4. Upper shoe has a convex surface to place on the concave surface of lower shoe.

Disc shaped roller bearing guide consists of 55 steel balls of 4 mm diameter, embedded within the bearing guides, for providing highly smooth surface in order to decouple the structure from the ground. Upper shoes, lower shoes and bearing guide were made of carbon steel (SC50C) and ball bearings were made of steel (SUJ2) material.

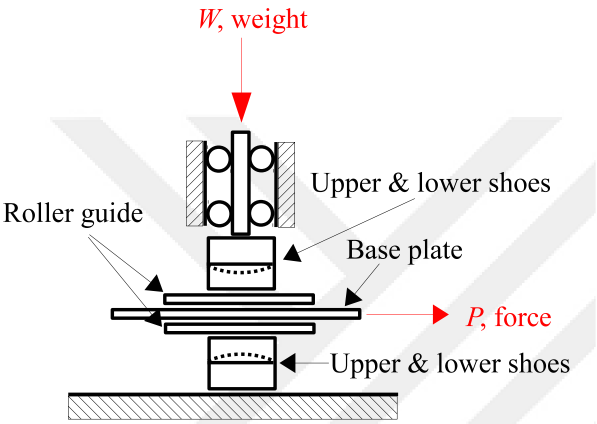

Figure 5.5: Friction test mechanism of roller bearings

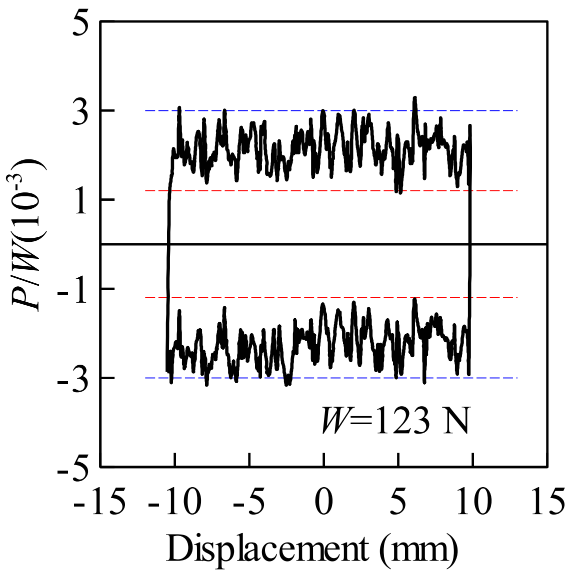

Figure 5.6: Frictional coefficient diagram

Figure 5.5 illustrates the friction test mechanism of roller bearings in order to obtain the frictional coefficient of the roller bearing guide. Here, a pair of upper shoe - lower shoe - roller guide were placed upside and underside of the base plate. Then the base plate was forced to move back and forth through electric activator while the mechanism was under loading weight. The displacement of the base plate was measured through a laser measurer. The frictional coefficient diagram which obtained under 123 N vertical loads, Figure 5.6, shows that the expected coefficient of the roller bearings was between 0.003 and 0.0012.

5.2.3 Viscous damping coefficient of additional dampers

In order to come up with affordable damping solution for the experimental vibration model, a viscous damper device was designed that consists of container with two silicon oil pools, connection plates and parallel plates as shown in Figure 5.7. Containers were attached to the fixed sub-frame whereas two pieces of connection plates were fixed to the movable sub-frame. And the parallel plates which assembled with connection plates were placed into the oil pools to make the connection between fixed and movable sub-structures. The dimensions of the container are $60 \times 150 \times 20$ mm (width $\times$ length $\times$ depth). The bottom surface of the parallel plates has 20 mm width and 110 mm length with 5 mm cut edge. So the bottom surface area of the parallel plates becomes $a = 2150$ mm^2. Each of these three parts was made of aluminium alloy.

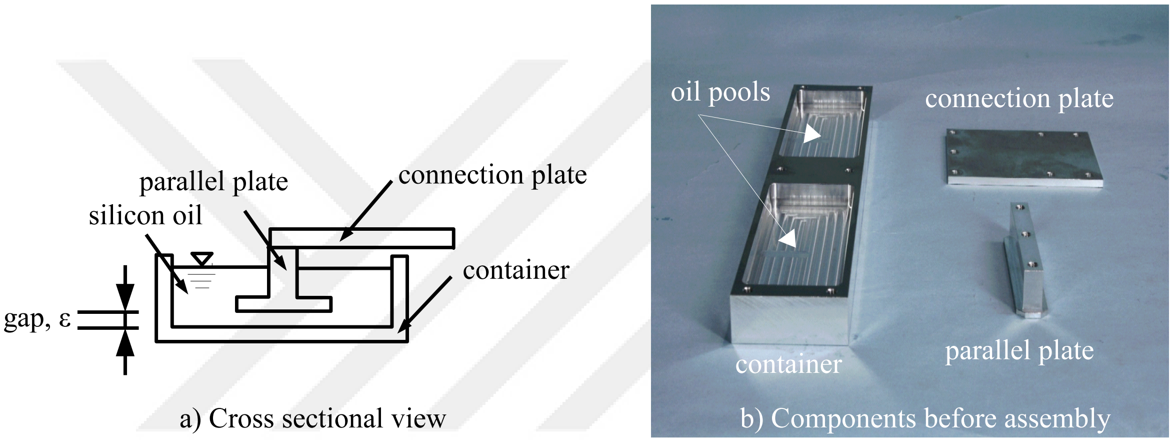

Figure 5.7: Viscous damper device

The viscous damping coefficient of the damper device was estimated by given formula as follows;

$$d' = 2\nu a/\varepsilon \tag{5.1}$$

, where ε is the gap between lower surface of the parallel plate and base surface of the container, a is the lower surface area of the parallel plate, ν is the dynamic viscosity of the silicon oil and d' is the viscous damping coefficient due to only one connection plate. Therefore the viscous damping coefficient becomes $d = 2\ d'$ for two connection plates.

The viscous damper was subjected to performance test to obtain the viscous damping coefficient. The container was forced to move back and forth in the vertical direction through electric activator and the reaction forces were obtained through load cell for different gaps as illustrated in Figure 5.8.a. The silicon oil has a $\rho = 3000$ mm^2/s of viscosity and $\mu = 970$ kg/m^3 of density and $\upsilon_{25^{\circ}C}$ = 2.91 Ns/m^2 of the viscosity coefficient for 25°C of room temperature. However the theoretical viscosity coefficient of the silicon oil was $\nu_{21^{\circ}C}$ = 3.14 Ns/m^2 for 21°C. Figure 5.8.b. shows the diagram of damping coefficient versus gap.

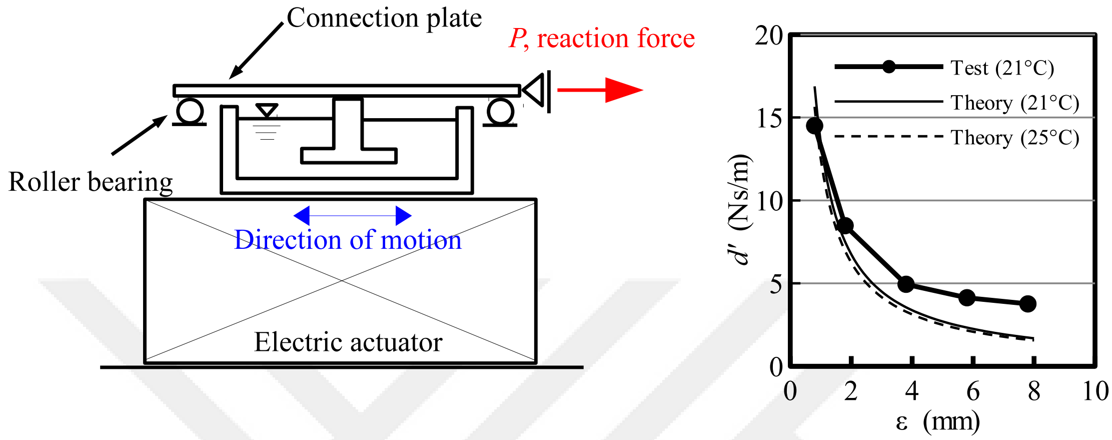

a) Test mechanism b) Damping coefficient diagram

Figure 5.8: Viscous damping coefficient test

5.3 Experimental studies

Since large additional dampers were added to the proposed structure for the case of vibration model with additional dampers, complex modes of experimental model due to obtained parameters in previous sections were calculated by using complex eigenvalue analysis, Foss Method [16]. Then a set of experiments to obtain dynamic parameters such as damping ratio and natural period, and elastic dynamic responses were conducted.

5.3.1 Free vibration analysis

Free vibration test is a perfect way to obtain realistic values for natural period and damping ratios of a structure when compared to simulations due to assumptions to be made during the idealization of numerical model. For this purpose, the vibration model was mounted on the shaking table. Then, the vibration model was manually induced for a few times laterally. The displacements were recorded during oscillation until it came to rest. This process was repeated for 10 times to get the results precisely. This test was conducted two times for the proposed vibration model with and without additional damper systems.

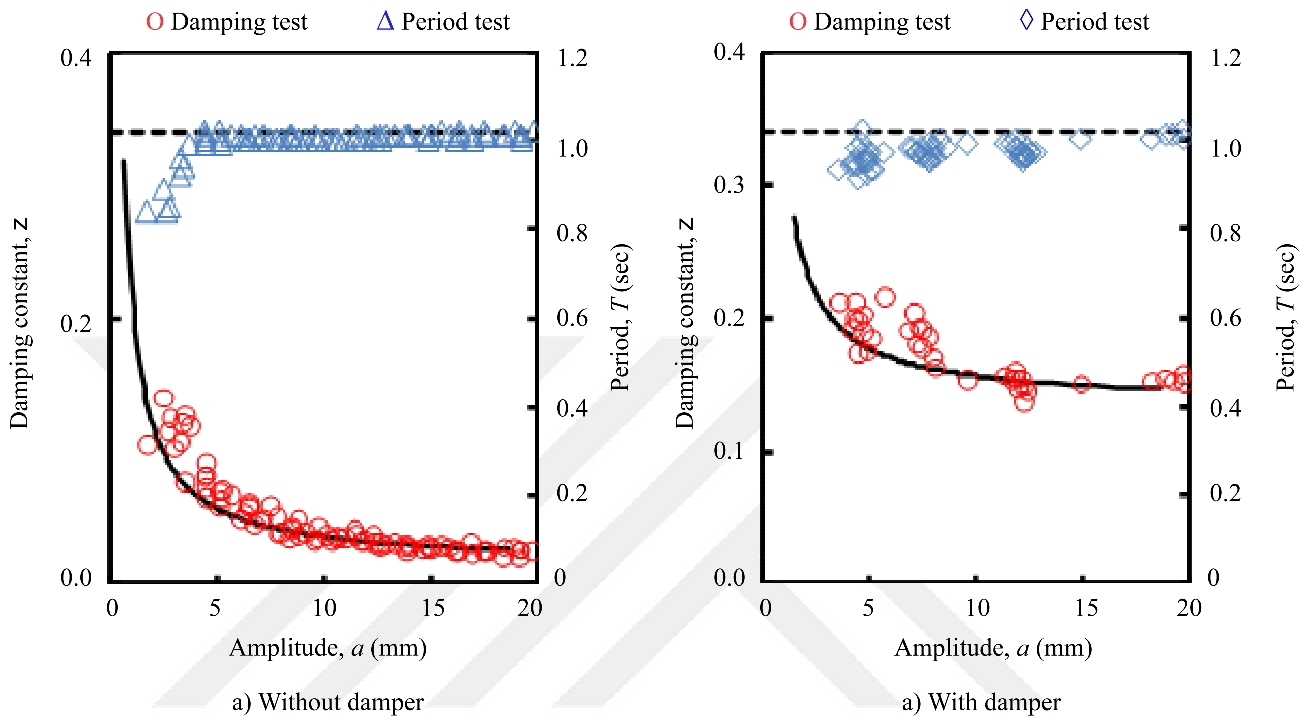

Figure 5.9: Natural period and damping tests of FCSS

The dynamic fictional force of the roller bearing system increases the damping of the structure. A frictional damping by a dynamic frictional force is evaluated so that the total energy dissipated per cycle is the same as for the viscous damping vibration during a steady state of motion. As the result this frictional damping can be evaluated by the following formula:

$$\zeta_e = 2f_b \times \frac{|\phi_{2n,i}|}{\pi\theta\omega_i} \times \frac{|\phi_{j,i}|}{a_j} \qquad (5.2)$$

, where ζ_e is called the equivalent viscous damping constant of the i-th natural vibration mode, θ and a_j are the frequency and the amplitude at beam-j during a steady state of motion, respectively. Damping constant ζ, can be estimated by addition of structural damping constant and equivalent viscous damping constant of the roller bearing support $\zeta_0 + \zeta_e$, due to friction forces.

Equivalent viscous damping constant can be calculated by Eq. 5.2 where, f_b is the frictional force at the roller bearing, θ_b is the amplitude of the equivalent vibration mode of the roller bearing, ω is the natural frequency, ϕ_i is the amplitude of the natural vibration mode, θ is the (circular) shape frequency of the observed object, a is the observed amplitude and natural vibration modes.

The total force and the friction coefficient at the roller bearing are 600N and 0.0012, respectively. Therefore the frictional force is equal to f_b = 0.0012×600N = 0.72N. As it seen in Figure 5.9 the damping constant decreased as long as the amplitude increased and in spite of the increasing amplitude value, the natural period changed in a small range. The structural damping constant of the vibration model was assumed as ζ_0 = 0.015. Besides, the viscous damping constant was d = 2×7.5 Ns/m = 15 Ns/m corresponding to the gap of 2 mm as seen from Figure 5.8.b. The damping constant of the additional viscous dampers and the natural period were obtained ζ = 0.135 and T_{d1} = 1.017 sec, respectively.

5.3.2 Elastic dynamic response analysis

The vibration model of the proposed structure with and without additional dampers were tested through shaking table, Figure 5.10, to verify the seismic response behaviour due to El Centro, Taft, Hachinohe and Miyagi earthquakes. The maximum acceleration of seismic waves was scaled to 300 gal when investigating the seismic behaviour of the proposed structure using 15-storey numerical model. This time, the maximum acceleration of the seismic waves used in shaking table test was set to 50 gal to avoid damages on experimental vibration model.

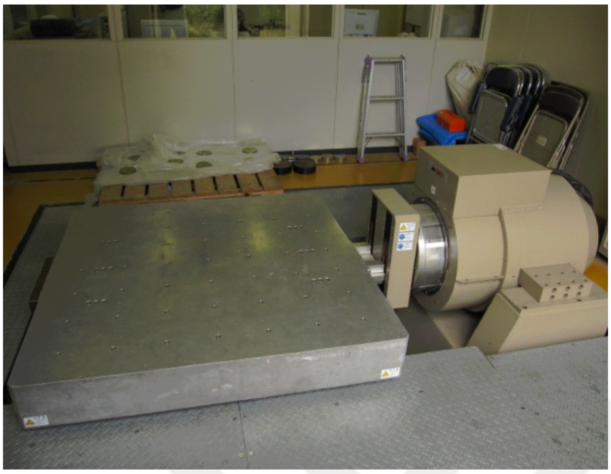

Figure 5.10: Shaking table and experimental model

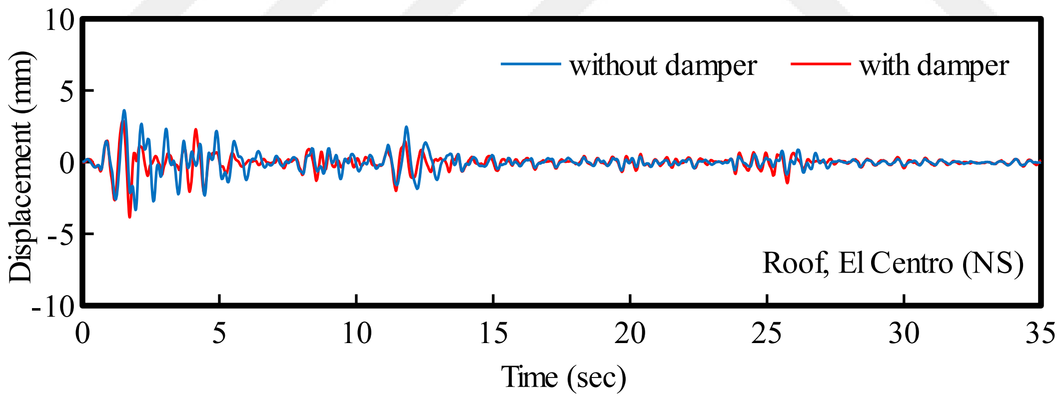

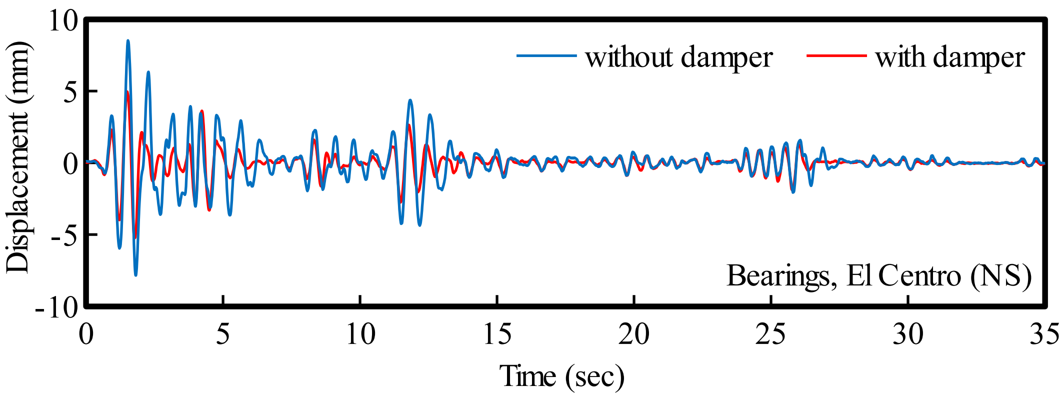

Figure 5.11: Shaking table responses of experimental model

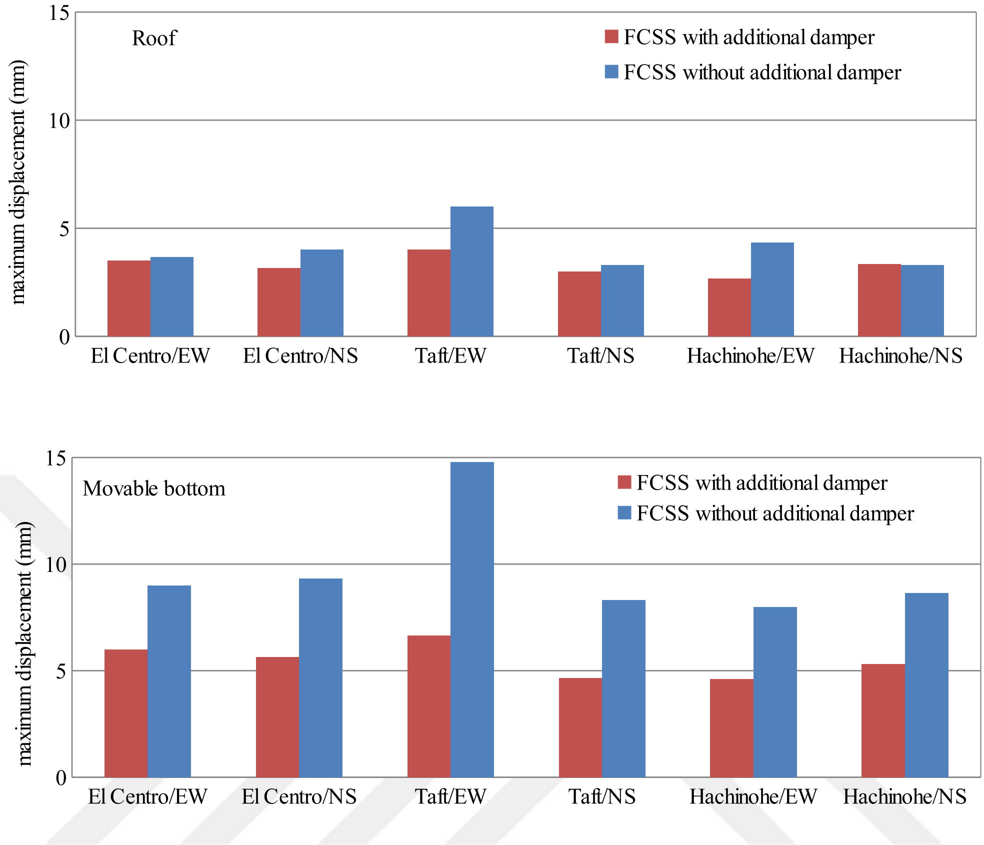

Figure 5.12: Maximum shaking table responses of experimental model

Similar to the numerical analysis, the responses for the proposed building was decreased. However, the displacement responses can be relatively higher for the vibration model when no additional dampers were used.

5.4 Computational verification of experimental vibration model

As it is mentioned before, the experimental vibration model is not a scaled model. It is needed to confirm that the behaviour of the experimental vibration model is consistent and accurate. Therefore, ABAQUS software, a well known and powerful finite element software, is chosen for the simulation studies of the proposed building especially for the dynamic analyse studies.

If we have a brief look at literature on the studies using ABAQUS software, it is seen that the program have became increasingly used recently especially in the field of earthquake engineering including base isolation system analysis, and contact simulations to get the most accurate result before production. On the other hand, since the program is so complicated the probability of making mistakes are much more simple.

Clarke *et al.* used ABAQUS software to model a real scale FPBs for an structural platform of an offshore structure. It is also noted that the software is more complex for the users when compared to special purpose software aiming structural analysing [17].

5.4.1 Eigenvalue analysis

After modelling experimental vibration model in ABAQUS software, Figure 5.13, eigenvalue analysis were conducted. The eigenvalue results of ABAQUS were compared to the results of experimental model that illustrated in Figure 5.9. Table. 5.1 shows that the first natural period of experimental model obtained in free vibration analysis is $T = 0.98$ sec, whereas the result for ABAQUS simulation is $T = 0.982$. The results are almost same for both case. The first, second and third vibration modes of the proposed model obtained by ABAQUS due to eigenanalysis, Figure 5.14.

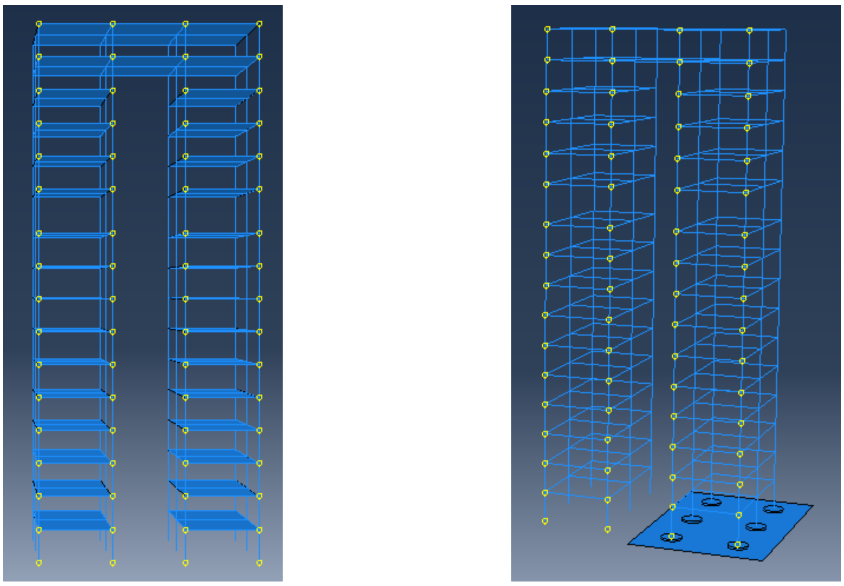

Figure 5.13: ABAQUS simulation of experimental model

Table 5.1: Eigenvalues of the experimental model

	Experimental model	ABAQUS result		
	First	First	Second	Third
$T(sec)$	0.98	0.982	0.308	0.181

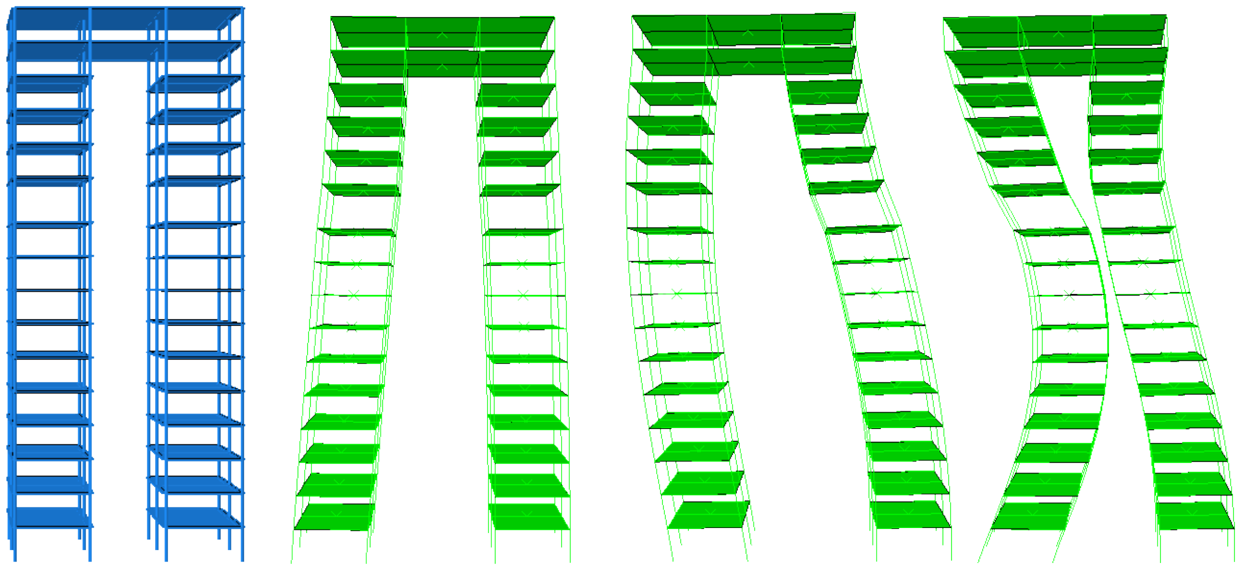

Figure 5.14: Vibration modes obtained by ABAQUS

5.4.2 Elastic dynamic response analysis

The seismic responses of the modified vibration model is also tested through shaking table test due to same earthquake waves 50 gal of maximum acceleration. It is seen in Figure 5.15 that the seismic responses for shaking table and computer simulations are in good match.

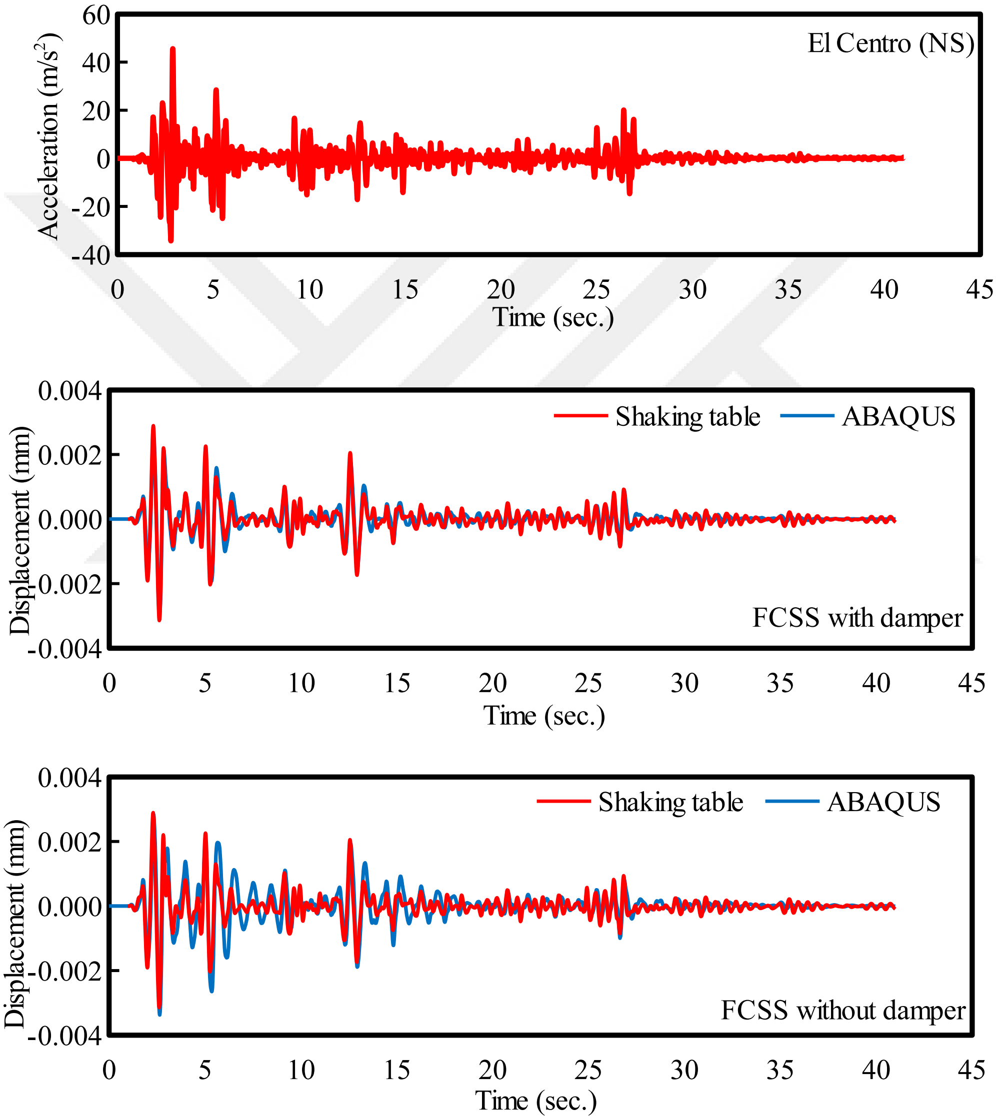

Figure 5.15: Comparison of shaking table test responses with ABAQUS

5.5 Conclusion

In this chapter, experimental studies using proposed folded cantilever shear structure model are conducted. Experimental model and vibration model components are introduced in terms of dynamic vibration characteristics. Experimental studies including free vibration test for natural period and natural damping analysis, and shaking table test for verifying the seismic characteristic behaviour of the proposed model are conducted. These results are also simulated in ABAQUS, a well known finite element software in order to confirm the results. Both experimental studies and the simulation results were obtained in good match.

CHAPTER 6

Modified Model of the Proposed Structure

6.1 Introduction

In this chapter, the structural configuration is modified for better use of proposed model. So far, both numerical and experimental study results were satisfying in terms of seismic performance for the proposed structure. However, it is considered that it is possible to increase the damper placement space with a simple modification that also provides structural regularity compared to first structural configuration of the proposed model.

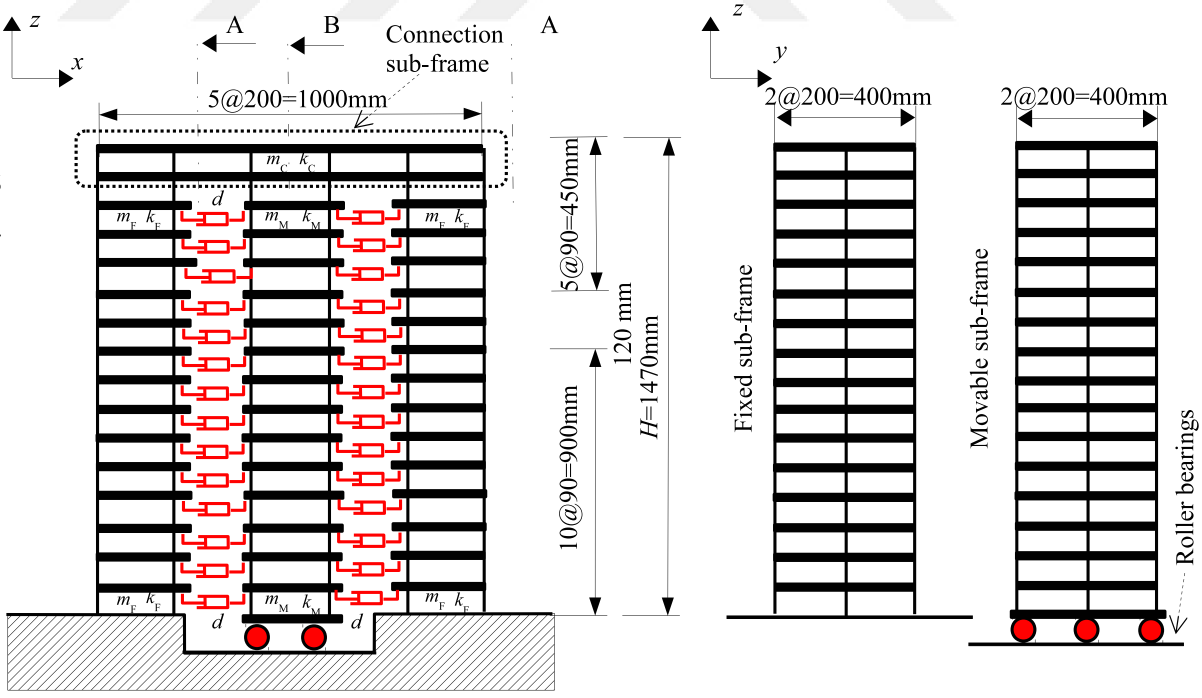

a) Front view

b) Side views

Figure 6.1: ABAQUS simulation of experimental model

Considering the middle point of movable sub-frame as a center of symmetry, the configuration is reformed by designing it as a symmetrical building. The structural configuration became like fixed-movable-fixed sub-frames order whereas the first configuration was like fixed-movable sub-frames order. Figure 6.1 illustrates the modified vibration model. Similar to the first configuration model in Figure 5.1, modified model is 16-storey. The beams was constructed by using 230 mm $\times$ 5 mm $\times$ 430 mm and 1030 mm $\times$ 5 mm $\times$ 430 mm sized rigid aluminium alloy (A5052) rectangular plates as beams for fixed - movable sub frames and connection sub-frame, respectively.

Figure 6.2: Modified experimental model

The clearance between columns was 200 mm along x and y directions. That is, the vibration model was 1000 mm in length and 400 mm in width. Experimental model components are identical to the previous model. That is, dynamic characteristics of these components are same with the previous model.

6.2 Computational verification of modified model

As like in previous chapter, the modified vibration model is simulated by using ABAQUS software. For this purpose, the eigenvalue analysis and shaking table test responses verified.

6.2.1 Eigenvalue analysis

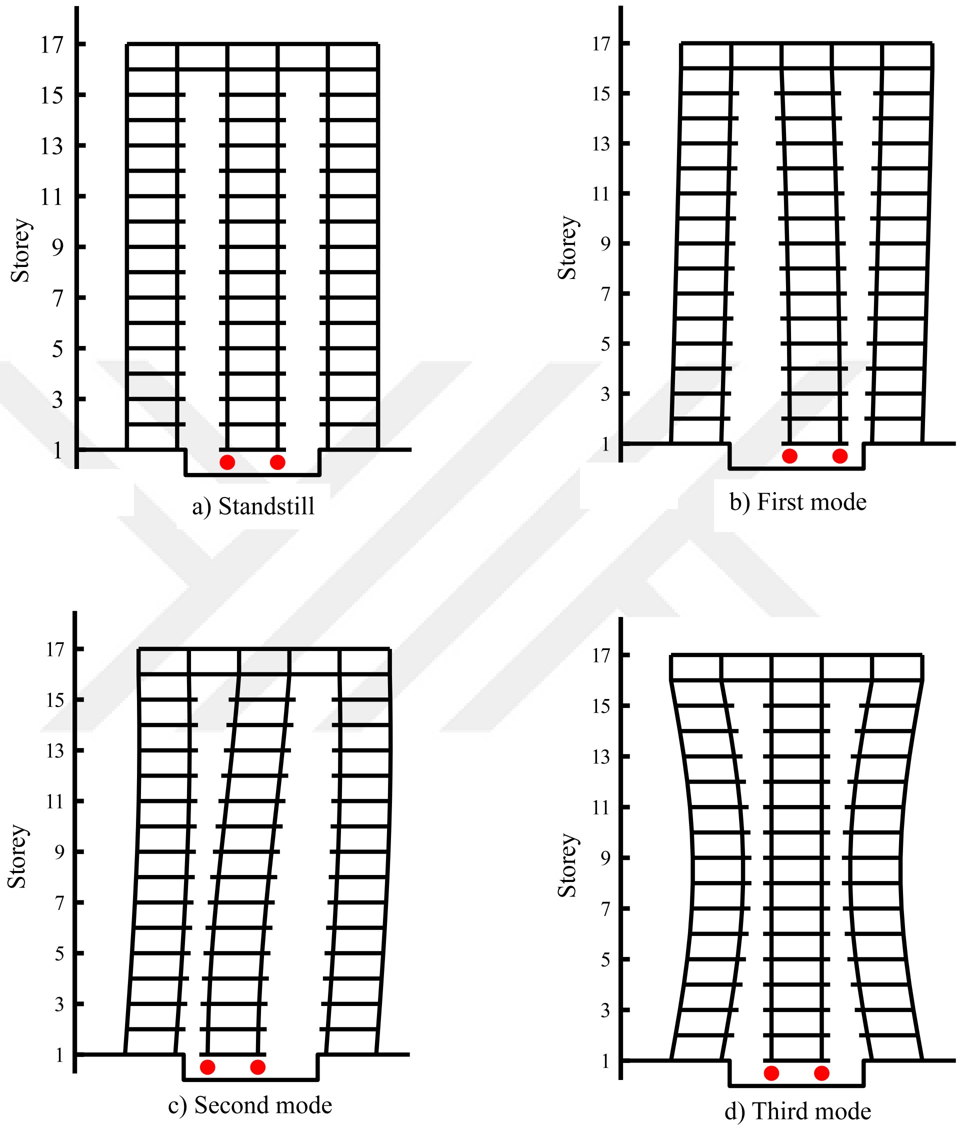

Figure 6.3: Vibration modes of System-O using Foss Method

The first, second and third natural periods were obtained 0.808, 0.458 and 0.429 for the modified experimental model. The natural period values were obtained 0.808, 0.330 and 0.199 for the ABAQUS model. The first, second and third natural frequencies were obtained 7.775, 13.69, 14.63 and 7.733, 19.01, 31.42 for the experimental and ABAQUS model, respectively.

Table 6.1: Complex eigenvalues of System-O and System-AD

	Shaking table	ABAQUS		
	First	First	Second	Third
$T(sec)$	0.808	0.808	0.330	0.199
$frequency$	7.775	7.733	19.01	31.42

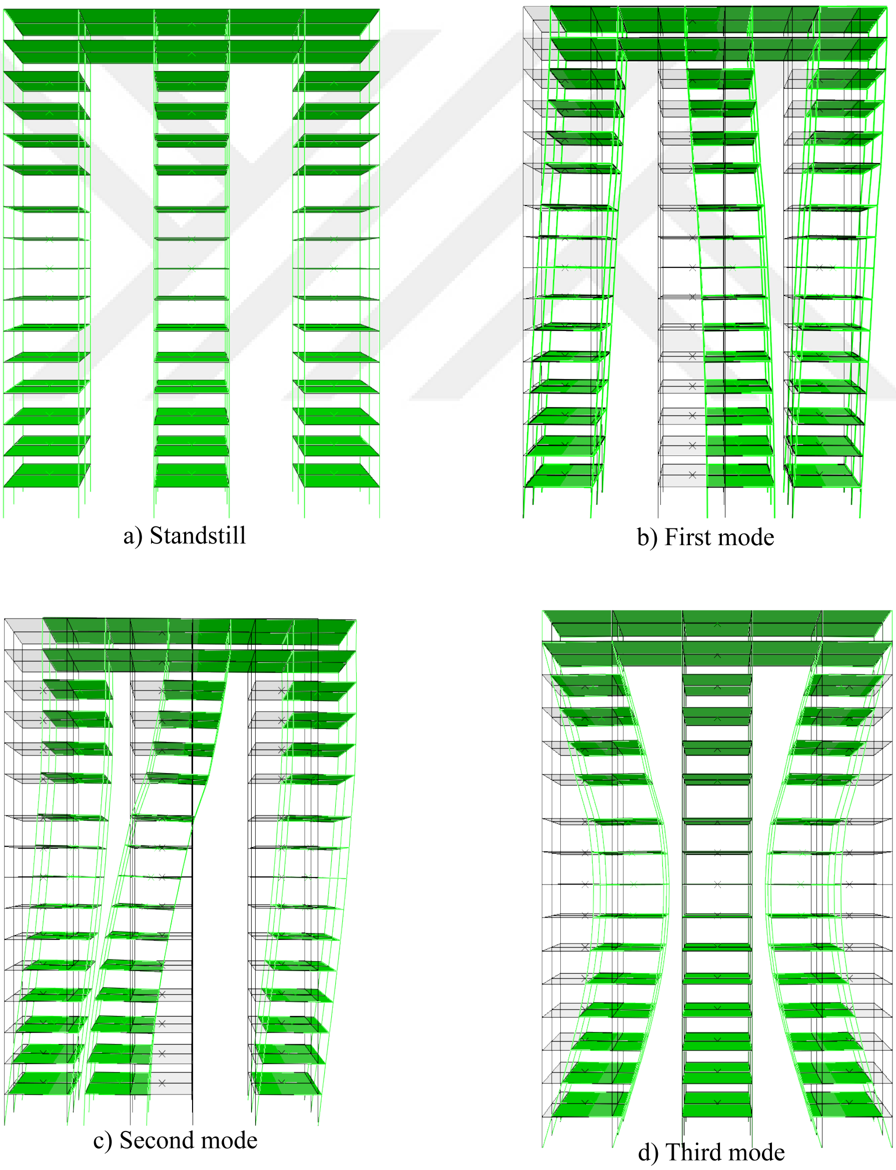

a) Standstill

b) First mode

c) Second mode

d) Third mode

Figure 6.4: Vibration modes of System-O using ABAQUS

6.2.2 Shaking table analysis

The seismic responses of the modified vibration model is also tested through shaking table test due to same earthquake waves. Similarly, the maximum acceleration of the seismic waves used in shaking table test was set to 50 gal to avoid damages on experimental vibration model.

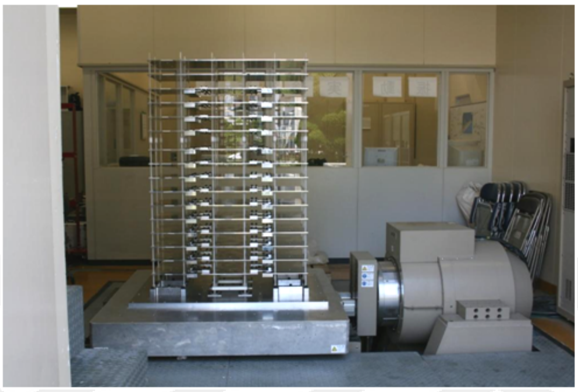

Figure 6.5: Modified model mounted on shaking table

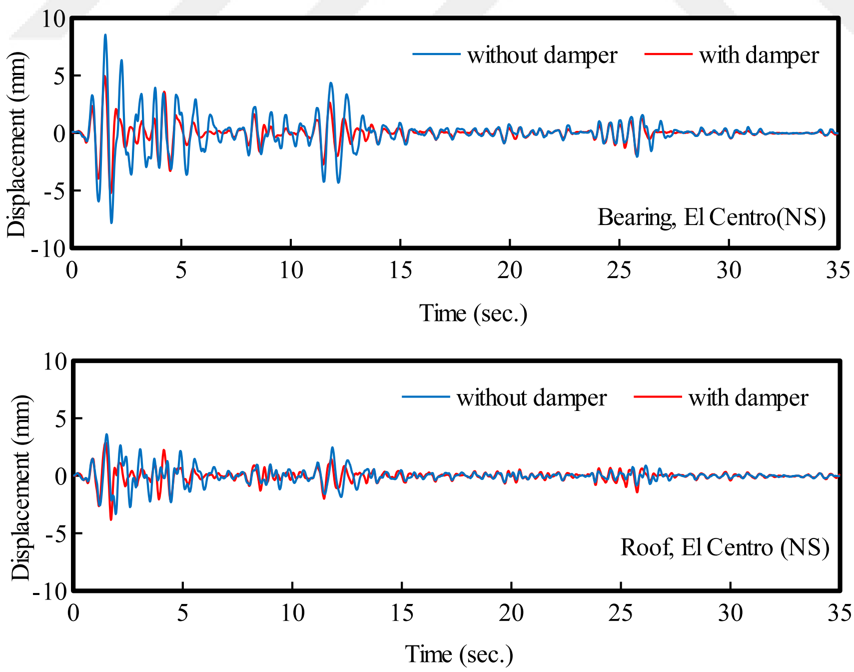

Figure 6.6: Seismic responses of modified model due to shaking table

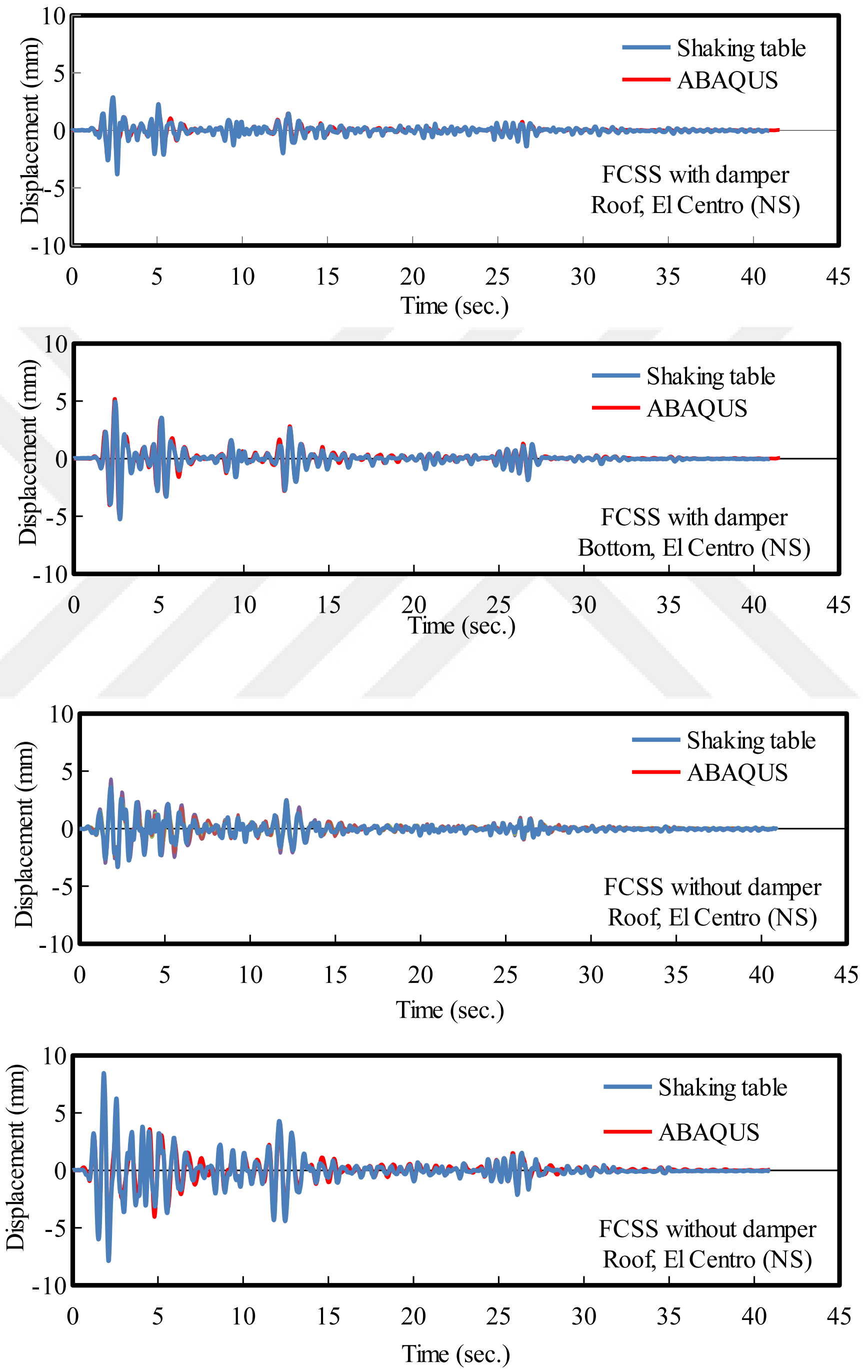

Figure 6.7: Seismic response comparison of modified model and ABAQUS

6.3 Real-scale building investigations

In this section, an illustrative example for a real-scale building is given. The model is 11-storey with 38.5 m of total height, each storey has a 3.5 m of storey. The masses are arranged to be $500,000$ kg for the ordinary building for each floor. As for proposed building, the mass is set to be $125,000$ kg, $250,000$ kg and $500,000$ kg for the fix, movable and connection sub-frames, respectively. Besides, the movable bottom floor is to be $500,000$ kg as well.

Table 6.2: Spring-mass model parameters

Parameter	Proposed Building	Ordinary Building
Total height, H	$38.5m$	$38.5m$
Number of stories, n	11	11
Storey height, h	$3.5m$	$3.5m$
Total mass, m	$6,000,000kg$	$5,500,000kg$
First structural damping ratio	$\zeta_1 = 2\%$	$\zeta_1 = 2\%$
Additional damping coefficient	$d_0 \sim d_15 = 0.25 \times 10^6 Ns/m$	–
First additional damping ratio	$\Delta\zeta_1 = 20\%$	–
Frictional coefficient	$\mu = 0.005$	–
Frictional force, N	$f = 159,250N$	–

According to the eigenvalue analysis results, the first natural period was obtained around 2.57 sec for the proposed. And the natural period of ordinary building was obtained around 1.16 sec.

Similar to the previous studies, elastic dynamic response analysis was conducted as well due to El Centro, Taft and Hachinoe earthquakes. In Figure 6.8, the maximum acceleration, maximum displacement and base shear coefficient responses are given. Maximum acceleration responses were obtained for ordinary building model, and the minimum responses for proposed building with additional dampers. As for displacements, the maximum values were obtained for the proposed building without additional dampers. Therefore, it is suggested to use proposed building with optimal damper placement between the beams against excessive displacements. Base shear responses were also obtained similar to the acceleration responses with maximum for ordinary, and minimum for proposed building model.

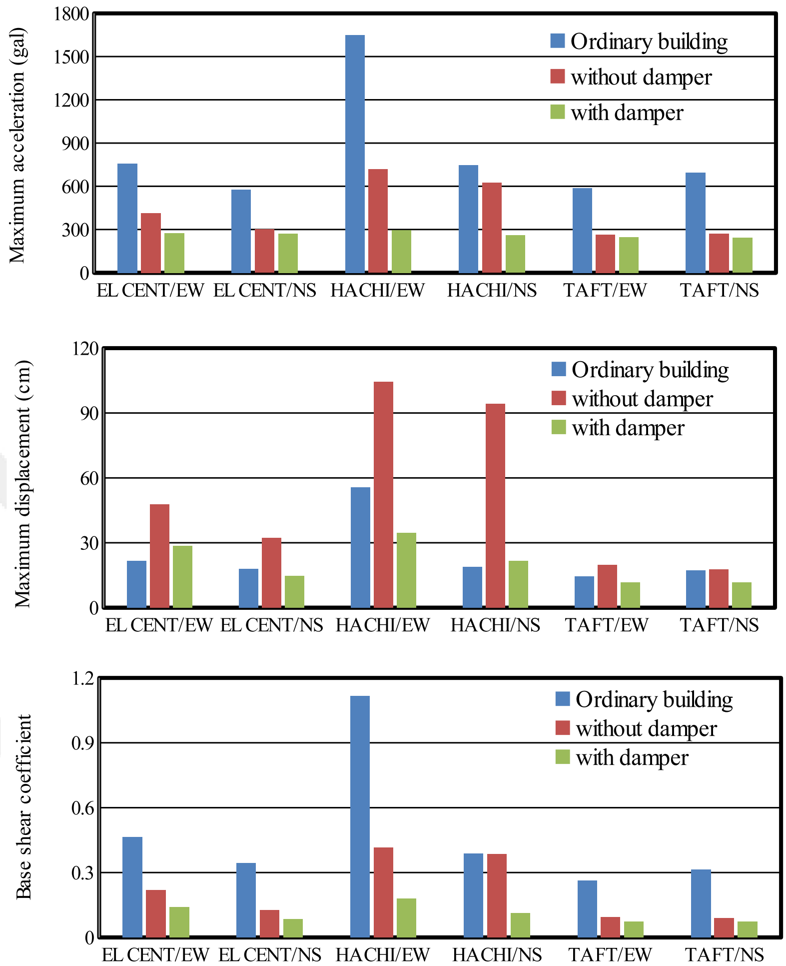

Figure 6.8: 11-storey real scale model responses

6.4 Conclusion

In this chapter, modified configuration for the proposed building is introduced with the aim of increasing the damper placement space and providing structural regularity for better use. Verification studies were conducted for eigenvalue analysis and dynamic response analysis. To set an example, a real-scale building of modified configuration is given. According to the results, obtained responses verifies the theory of the proposed model which also performed satisfying results on numerical and experimental studies.

CHAPTER 7

Conclusion and Discussion

In this dissertation, the newly designed folded cantilever shear structure was investigated through numerical and experimental studies with the aim of increasing the natural period and damping ratio to reduce seismic responses. For this purpose, a new seismic isolation approach was proposed incorporating base isolation system and coupling method into a mid-rise structure. A new configuration for buildings of similar heights has been studied by connecting them at the roof part. The boundary conditions were selected to be one fixed supported building and the other one to be base isolated building while using rigid connection element at the top part. Based on the results, it was found that: 1) Coupling method was effective to incorporate base isolated and fixed supported frames in a building of similar heights by means of rigid connection sub-frame at the top part. 2) Proposed building is capable of extending the natural period two times compared to ordinary structure, which has the same number of storey, by increasing floor number two times without changing neither the total height of structure nor the number of storey. 3) The relative displacements with respect to the base of the proposed structure were relatively higher compared to ordinary building. Therefore, additional viscous dampers attached between sub-frames, and proposed structure with additional viscous dampers resulted in satisfying seismic performance. 4) The relative displacements with respect to the base of the proposed structure were relatively higher compared to ordinary building. Therefore, additional viscous dampers attached between sub-frames, and proposed structure with additional viscous dampers resulted in satisfying seismic performance.

The proposed structure was modified to avoid structural irregularity with a symmetrically designed building of fcss consisted of non-isolated - fully isolated - non-isolated sub-frame configuration. In general terms, the modified structure provided better outcomes such as symmetrical configuration, providing more space for damping placement and better seismic performance.

Bibliography

[1] K. Ohami, S. Otani, and S. Abe, "Seismic Retrofit by Connecting to Adjacent Building," in *the Proceeding of the 14th World Conference on Earthquake Engineering*, 2008.

[2] Y. Azuma, S. Otani, and K. Ohami, "Seismic Response Control by Interconnecting Adjacent Buildings-Feasibility Study," in *The Proceeding of the 4th international Conference on Earthquake Engineering*, no. 188, 2006.

[3] C.-L. Ng and Y.-L. Xu, "Seismic Response Control of a Building Complex Utilizing Passive Friction Damper: Experimental Investigation," *Earthquake Engineering & Structural Dynamics*, vol. 35, pp. 657–677, May 2006.

[4] Y. Xu, Q. He, and J. Ko, "Dynamic Response of Damper-Connected Adjacent Buildings Under Earthquake Excitation," *Engineering Structures*, vol. 21, pp. 135–148, Feb. 1999.

[5] J. Luco and F. D. Barros, "Optimal Damping Between Two Adjacent Elastic Structures," *Earthquake Engineering & Structural Dynamics*, vol. 27, pp. 649–659, 1998.

[6] G. Cimellaro and M. D. Angelis, "Theory Ed Experimentation on Passive Control of Adjacent Structures," in *The Proceeding of the 13th World Conference on Earthquake Engineering*, no. 1837, 2004.

[7] T. Aida, T. Aso, K. Takeshita, T. Takiuchi, and T. Fujii, "Improvement of the Structure Damping Performance By Interconnection," *Journal of Sound and Vibration*, vol. 242, pp. 333–353, Apr. 2001.

[8] M. Basili and M. De Angelis, "A Reduced Order Model for Optimal Design of 2-Mdof Adjacent Structures Connected by Hysteretic Dampers," *Journal of Sound and Vibration*, vol. 306, pp. 297–317, Sept. 2007.

[9] V. Agarwal, J. Niedzwecki, and J. van de Lindt, "Earthquake Induced Pounding in Friction Varying Base Isolated Buildings," *Engineering Structures*, vol. 29, pp. 2825–2832, Nov. 2007.

[10] M. M. Abdullah, J. H. Hanif, A. Richardson, and J. Sobanjo, "Use of a Shared Tuned Mass Damper (STMD) to Reduce Vibration and Pounding in Adjacent Structures," *Earthquake Engineering & Structural Dynamics*, vol. 30, pp. 1185–1201, Aug. 2001.

[11] A. Hayashi, "Development of Response Controlled and Linked Structural System in Over Track Buildings," 2007.

[12] K. Iwasaki, A. Hayashi, and T. Masuda, "Study of Practical Application of Seismic Reinforcement Method for Over-track Station Buildings Using Adjacent Buildings," 2009.

[13] D. L. Garcia, "A Simple Method for the Design of Optimal Damper Configurations in MDOF Structures," *Earthquake spectra*, 2001.

[14] J. K. Whittle, M. S. Williams, T. L. Karavasilis, and A. Blakeborough, "A Comparison of Viscous Damper Placement Methods for Improving Seismic Building Design," *Journal of Earthquake Engineering*, vol. 16, pp. 540–560, May 2012.

[15] "The Standard Building Law of Japan, Notifications of MLIT," tech. rep., 2009.

[16] K. Foss, "Coordinates Which Uncouple the Equations of Motion of Damped Linear Dynamic Systems," *Journal of Applied Mechanics*, vol. 32, no. 3, pp. 361–364, 1958.

[17] C. Clarke and R. Buchanan, "Structural Platform Solution for Seismic Arctic Environments-Sakhalin II Offshore Facilities," 2005.

APPENDIX A

Appendix